TAMPEREEN TEKNILLINEN YLIOPISTO
TAMPERE UNIVERSITY OF TECHNOLOGY

JIRKA YLÖNEN

ELECTROMYOGRAPHIC ARTEFACTS IN ELECTROENCEPHALOGRAPHIC MEASUREMENTS

Master of Science thesis

Examiners: Professor Hannu Eskola
and Professor Ilpo Vattulainen
Examiners and topic approved by
the Faculty Council of the Faculty of
Computing and Electrical
Engineering
on 4th February 2015

ABSTRACT

JIRKA YLÖNEN: Electromyographic Artefacts in Electroencephalographic Measurements
Tampere University of technology
Master of Science Thesis, 66 pages
September 2015
Degree Program in Electrical Engineering
Major: Technical Physics
Examiners: Professor Hannu Eskola and Professor Ilpo Vattulainen

Keywords: EEG, EMG

Recording electroencephalogram (EEG) is a common medical examination, which is commonly used in the diagnosis of epilepsy. Movements or tension of muscles, especially in the facial area, create electromyographic (EMG) signals, which often appear in EEG recordings. EMG artefacts hinder the interpretation of EEG, and because they are often located in the same frequency band as the actual EEG, they cannot be simply filtered away.

In this Master's thesis, completed at the Department of Clinical Neurophysiology at Seinäjoki Central Hospital, and at the Department of Electronics and Communications Engineering at Tampere University of Technology, the aforementioned EMG artefacts were investigated. The ultimate objective was to identify the frequency bands from the measured EEG signal where the actual EEG data and EMG artefacts are located and if occurring at the same frequency range identify and separate the EMG artefact from the EEG signal. One of the objectives was also to determine the muscular origin of EMG artefacts. Within the framework of this Master's thesis, EEG and facial EMG from several muscles (frontalis, temporalis and masseter) were recorded simultaneously, under the condition of tensed muscles. Using these signals, frequency responses were calculated maintaining the tissues between EMG and EEG channels as a digital filter. A simulated facial EMG was utilized with a measured frequency response to simulate an EMG artefact. The simulated artefact was applied to EEG channels. The conduction of facial EMG signal to EEG channels was then analyzed using a simple spherically symmetric volume conductor model. Results obtained from the model were compared to results obtained from recordings.

A comprehensive solution to the objective of separating EMG artefacts from the EEG signal was not directly achieved in the current project. Based on the calculated frequency responses, results suggest that a peak occurs at frequencies below 100 Hz, where signal between EMG and EEG channels attenuates least. Simulated signals are not necessarily the most informative result of the current project, but they could become a future focus area for separating EMG artefacts. The spherical model used for modeling of the head proved to be insufficiently precise for the description of signal conduction in tissues. Thus, in the future it would be worthwhile to obtain a more complete head model, e.g. produced from an MRI image. With the help of an accurate

model, the inverse problem (resolving the EMG source computationally when the EMG artefact is known) could also be addressed.

TIIVISTELMÄ

JIRKA YLÖNEN: Elektromyografiset artefaktat elektroenkefalografisissa mittauksissa
Tampereen teknillinen yliopisto
Diplomityö, 66 sivua
Syyskuu 2015
Sähkötekniikan koulutusohjelma
Pääaine: Teknillinen fysiikka
Tarkastajat: professori Hannu Eskola ja professori Ilpo Vattulainen

Avainsanat: EEG, EMG

EEG:n eli aivosähkökäyrän rekisteröinti on yleinen lääketieteellinen tutkimus, jota käytetään erityisesti epilepsian diagnosoimiseen. Usein käyrässä esiintyy lihas- eli EMG-artefaktoja, jotka johtuvat siitä että potilas liikuttaa tai jännittää lihaksiaan, erityisesti kasvojen alueella. EMG-artefaktat haittaavat EEG:n tulkitsemista, ja koska ne usein esiintyvät samalla taajuusalueella varsinaisen aivosähkökäyrän kanssa, niitä ei pystytä yksinkertaisesti suodattamaan pois.

Tässä Seinäjoen keskussairaalan kliinisen neurofysiologian osastolla ja Tampereen teknillisen yliopiston Elektroniikan ja tietoliikennetekniikan laitoksella tehdyssä diplomityössä tutkittiin mainittuja EMG-artefaktoja. Pohjimmainen tavoite olisi selvittää, millä taajuusalueilla mitatussa EEG-signaalissa esiintyy varsinaista EEG:tä ja millä EMG-artefaktaa, ja pystyä erottamaan EEG ja EMG jos ne esiintyvät samalla taajuusalueella. Kiinnostavaa olisi myös tietää, mistä lihaksesta EMG-artefakta on lähtöisin. Diplomityön puitteissa ongelmaa lähestyttiin niin että rekisteröitiin samanaikaisesti EEG ja kasvo-EMG muutamasta lihaksesta (frontalis, temporalis ja masseter) silloin, kun niitä jännitettiin. Näitä signaaleja käyttäen laskettiin taajuusvasteet pitäen kudoksia EMG- ja EEG-kanavien välillä digitaalisena suotimena. Kasvo-EMG:tä myös simuloitiin, ja simuloidun EMG:n ja taajuusvasteiden avulla muodostettiin simuloitua EMG-artefaktaa EEG-kanaviin. Lisäksi kasvo-EMG:n leviämistä EEG-kanaviin tutkittiin yksinkertaisen pallosymmetrisen tilavuusjohdemallin avulla. Mallin antamia tuloksia verrattiin rekisteröinnin antamiin tuloksiin.

Työssä ei suoraan onnistuttu vastaamaan kysymykseen EMG-artefaktan erottamisesta EEG-signaalista. Lasketuista taajuusvasteista voidaan kuitenkin lähes varmuudella sanoa, että alle 100 Hz taajuudella esiintyy huippu, jossa signaali vaimenee EMG- ja EEG-kanavien välillä vähiten. Simuloidut signaalit eivät sinällään ole tutkimustulos, mutta niitä voitaisiin hyödyntää jatkossa EMG-artefaktan erottamiseen. Pään mallinnukseen käytetty pallomalli osoittautui liian epätarkaksi kuvaamaan signaalin johtumista kudoksissa. Tämän vuoksi kannattaisikin jatkossa käyttää realistista, esimerkiksi MRI-kuvasta saatua pään mallia. Sen avulla voitaisiin suoran ongelman lisäksi tutkia myös käänteistä ongelmaa, toisinsanoen tilannetta jossa EMG-artefakta EEG-kanavassa tunnetaan, ja EMG-lähde pyritään laskennallisesti selvittämään.

PREFACE

This Master's Thesis has been carried out at the Department of Clinical Neurophysiology at Seinäjoki Central Hospital, and at the Department of Electronics and Communications Engineering at Tampere University of Technology.

I wish to thank my supervisors, Ward Chief Physician Ville Jäntti and Chief Physicist Antti Kulkas, and examiners, Professor Hannu Eskola and Professor Ilpo Vattulainen. I'm grateful also to the nurses who assisted in the experimental part of the work, and Professor Jari Hyttinen, who appointed me to this project. Thanks also for the good advice from researchers in the Department of Electronics and Communications Engineering, specifically Narayan Puthanmadam Subramaniyam, Markus Hannula, Jarno Tanskanen and Atte Joutsen.

Tampere, 14.9.2015

Jirka Ylönen

CONTENTS

LIST OF FIGURES

LIST OF SYMBOLS AND ABBREVIATIONS

ACh	Acetylcholine
AP	Action potential
APR	Action potential rate
ATP	Adenosine triphosphate
C1-C8	Cervical nerves 1-8
CCA	Canonical correlation analysis
CN	Cranial nerve
DFT	Discrete Fourier transform
ECG	Electrocardiography
ECoG	Electrocorticography
EDF	European Data Format
EEG	Electroencephalography
EMG	Electromyography
ENG	Electroneurography
ENMG	Electroneuromyography
EOG	Electrooculography
EP	Evoked potential
EPP	End-plate potential
EPSP	Excitatory postsynaptic potential
fEMG	Facial EMG
FDM	Finite Difference Method
FEM	Finite Element Method
FFT	Fast Fourier transform
FIR	Finite impulse response
ICA	Independent component analysis
IDFT	Inverse discrete Fourier transform
IFFT	Inverse fast Fourier transform
IIR	Infinite impulse response
IPSP	Inhibitory postsynaptic potential
LMN	Lower motor neuron
MN	Motor neuron
MU	Motor unit
MUAP	Motor unit action potential
MUAPT	MUAP train
nEMG	Needle EMG
NMJ	Neuromuscular junction
PSP	Postsynaptic potential
REM	Rapid eye movement
RI	Responsiveness Index
SCG	Superior cervical ganglion
sEMG	Surface EMG
SR	Sarcoplasmic reticulum
UMN	Upper motor neuron

1. INTRODUCTION

The brain is essentially an electrical organ, and because tissues are conductive, electric activity of the brain can be recorded from the scalp. This method, called electroencephalography (EEG), was invented in 1924 by German neurologist Hans Berger and in modern times has become a common medical examination. Generally, 21 electrodes (channels) are attached to the patient's scalp, from which time-dependent potential signals are recorded. EEGs can be used for diagnosing many neurological conditions which cause changes to electrical activity of the brain; the most important application, however, is diagnosing epilepsy. In previous eras of medicine, EEGs have also been important in diagnosing brain tumors, but development of medical imaging methods has reduced its applications in this field. [4]

Disturbances often occur, or in medical terms, EEG artefacts. One of the most common artefacts is the electromyographic (EMG) artefact, which occurs if the patient moves or tenses muscles, especially in the facial area. This is explained by the fact that commands to move muscles proceed from brain to muscles electrically, specifically via so called action potentials. Because of tissue conductivity these action potentials are then recorded on the scalp as an EMG artefact. It's important to mention that EMG is also a medical examination, which is used for investigating electric activity of the muscles. EMGs can be recorded from the surface of the skin or directly from muscle with a needle. [4]

EMG artefacts hinder the interpretation of EEG signals, so the patient is asked to be still with muscles relaxed during EEG recording. It's usually impossible to completely eliminate them; this is problematic in small children and patients unable to remain still due to their condition. Afterwards, it is possible to remove EMG artefacts by the means of signal processing. The ultimate aim would be to solve, in which frequency bands in measured EEG signal the actual EEG occurs, similarly, the frequency bands where the EMG artefacts are located. This would make it possible to distinguish and separate EEG and EMG signals when they occur in same frequency band. It would also be useful to identify the muscular origin of the EMG artefact. [4]

In this Master's Thesis, carried out at Department of Clinical Neurophysiology at Seinäjoki Central Hospital, and at the Department of Electronics and Communications Engineering of Tampere University of Technology, EMG artefacts are investigated. The thesis is divided into scientific background and experimental sections. In the scientific background, the anatomy and physiology of muscles and motor neurons is introduced, specifically with relevance to the facial area. Basics of EMG and EEG are covered, as

well as a mathematical background for the processing of these signals. The advanced signal processing topic of EMG decomposition is also introduced, and continues to a discussion of how to simulate an EMG signal. A final topic is volume conductor modeling, which is presented briefly.

In the experimental section, EEG and needle EMG were recorded simultaneously from several facial muscles (frontalis, temporalis and masseter), with calculated frequency responses, monitored with tissues between EMG and EEG channels serving as a digital filter. In this task it's essential to detect and average motor unit action potentials (MUAPs) of single motor unit, as to cancel out EMG signal originating outside the measurement point cancels out. Since EMG signal usually contains MUAPs of several motor units, EMG decomposition algorithms become useful here. As mentioned earlier, the motor unit consists of group of muscle fibers and a motor neuron which innervates them, whereas MUAP is sum of action potentials of muscle fibers belonging to same motor unit.

The EMG signal was also simulated, and its simulated artefact was applied to EEG channels with the assistance of calculated frequency responses. Moreover, a simple spherical head model was constructed with COMSOL Multiphysics and potentials in EEG channels were calculated with the help of recorded EMG signals. These were then compared to potentials obtained from recorded EEG signals. Before the start of the project, it was known that it would have been preferable to use a more realistic head model obtained e.g. from MRI image. Due to the size of such a task and correspondingly lengthy computation times this was omitted.

An issue not covered in this Master's Thesis is the process of separating EMG artefacts from the EEG signal when the EMG source is unknown. One method is to calculate the entropy. Signal entropy, named after thermodynamic entropy, measures signal complexity and is larger if there's an EMG artefact in the signal. It has been used especially during anesthesia and sedation monitoring [8] [32]. A newer method, used also in monitoring, is the Responsiveness Index (RI) algorithm [33][34][35]. It's good to also mention ICA (Independent component analysis), which has been recently applied in EMG artefact separation [36]. It's a statistical method and one case of blind source separation [6].

2. BACKGROUND

In this chapter, the anatomy and physiology of the muscles and motor neurons is discussed. Skeletal muscles are the focus of this section, but cardiac and smooth muscles are discussed shortly. Muscles in the head area and their innervation are covered closely. Later, two important biophysical signals, electromyogram (EMG) and electroencephalogram (EEG) are discussed, including artefacts occurring in EEG. A mathematical background for processing EMG and EEG signals is covered, and from advanced signal processing, EMG decomposition with leader-follower clustering algorithm. EMG signal simulation is also discussed. Lastly, volume conductor modeling is shortly introduced, where the finite difference method (FDM) or finite element method (FEM) are generally utilized.

2.1 Muscles and motor neurons

Muscles consist of muscle cells (myocytes), which are also called muscle fibers. The diameter of skeletal muscle fibers (Figure 1) is 10 – 100 µm, but length, depending on the muscle, can be up to 30 cm. They are distinct from other cells in that they are multinucleate, containing many nuclei. Most of the space within the cells is filled by rod-like myofibrils, which are divided in transverse direction by Z discs into ~2 µm long sarcomeres. Sarcomeres consist of myofilaments. Thick myofilaments primarily contain myosin, and thin myofilaments primarily contain actin. Thick and thin myofilaments can slide along each other, which mechanically allows for muscle contraction. [2]

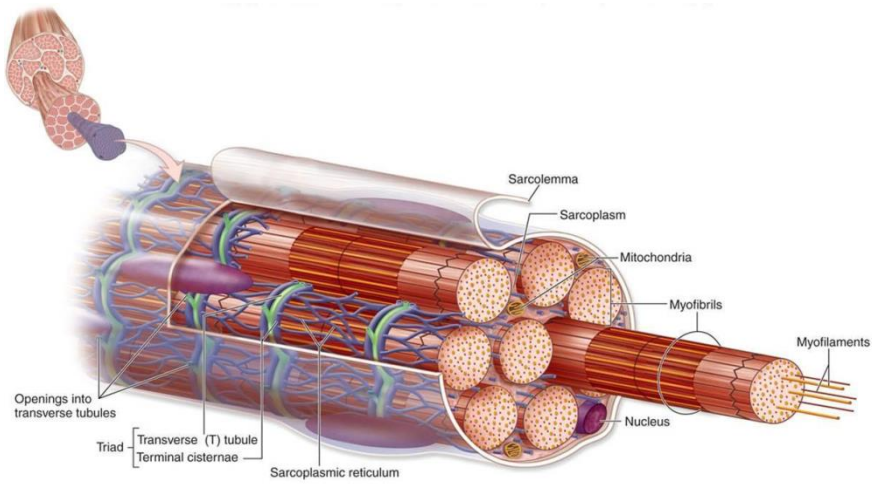

Figure 1. *Skeletal muscle fiber. [22]*

Cardiac muscle fibers resemble skeletal muscle fibers, but they are only 50-100 µm long and branched, joining each other in intercalated discs. They are also mononuclear. Both skeletal and cardiac muscles are called striated muscles, because single sarcomeres are clearly visible under a microscope. Instead, smooth muscle fibers resemble other cells of the body. They are small, mononuclear and have no myofibril and sarcomere structure. Their contraction is also based on myosin and actin myofilaments, but these filaments have an irregular arrangement. Smooth muscle fibers are connected to each other via gap junctions. [2]

Muscles are innervated by motor neurons (MN), where somatic motor neurons innervate skeletal muscles and autonomic motor neurons innervate cardiac and smooth muscles. Somatic motor neurons are divided into upper motor neurons (UMN) and lower motor neurons (LMN). Upper motor neurons, which begin from motor cortex of the brain, belong to central nervous system. Lower motor neurons belong to the peripheral nervous system, connecting cranial nerves and the peripheral regions of the body to the spinal nerves. Upper and lower motor neurons are joined via synapses in cranial nerve nuclei (cranial nerves), or in the ventral horn of the spinal cord (spinal nerves). Lower motor neurons join muscle fibers at neuromuscular junctions (NMJ). Almost all motor neurons have their axons covered by a myelin sheath. This sheath consists of glial cells, oligodendrocytes in the central nervous system (in UMNs) and Schwann cells in the peripheral nervous system (in LMNs). Between the glial cells there are unmyelinated gaps in the axon called nodes of Ranvier. Axons are also unmyelinated near the neuromuscular junction. A single motor neuron innervates several muscle fibers, and together the neuron and muscle fibers form a motor unit (MU). The amount of fibers in MUs is lowest in small muscles, for example in the eye, and highest in large muscles producing more force, e.g. in the legs. In the autonomic nervous system there are two lower motor neurons, which join to each other via

synapses in autonomic ganglia. In the heart, the postganglionic neurons join to cardiac muscle fibers at neuromuscular junctions, even if only a few so called pacemaker cells are directly innervated. In smooth muscle tissue, there are no neuromuscular junctions, but instead bulbous swellings called varicosities in the axon of the postganglionic neuron. The area between varicosities and muscle fibers can be also called a diffuse junction. [2]

At a resting state there's about -70 mV potential between the inside outside of the motor neuron (negative voltage corresponds to lower potential). This membrane potential occurs in fact in all cells, and comes from concentration gradients of ions inside and outside of the cell. The most important ions are K^+ (which has high concentration inside the cell and low concentration in extracellular space) and Na^+ and Cl^- (which have high concentration outside the cell and low inside the cell). Differences in ion concentrations tend to stabilize due to diffusion and electric field created by the presence of the ions. This process is slow, however, because permeability of the cell membrane is relatively low for all ions, with slight variation between them. Differences in concentration are also maintained by another mechanism, which is carried out by Na^+/K^+ pumps. They are protein structures in the cell membrane which pump Na^+ ions out of the cell and K^+ ions into the cell using ATP as energy source. [2][4]

Signals in motor neurons (like in all neurons) are propagated via action potentials (APs). An action potential begins when membrane potential depolarizes (becoming less negative). This opens Na^+ channels at the cell membrane; when Na^+ ions flow fast into the cell, further depolarization occurs and shifts the potential to positive. After about one millisecond, Na^+ channels are closed, but K^+ channels are opened. At this point, K^+ ions flow quickly out of the cell, returning membrane potential to negative again (repolarization), and to slightly more positive levels than the pre-AP potential (hyperpolarization). At last, K^+ channels are closed, and Na^+/K^+ pumps return ion concentrations and membrane potential to their original state. The period when membrane potential differs from normal potential during action potential is called the refractory period. The period of depolarization and repolarization phases is called the absolute refractory period, because during which it's impossible to generate a new action potential. The period when membrane potential returns from a hyperpolarized state to its original state is called the relative refractory period, because it's possible to generate new action potential during it, but the stimulus must be stronger than normal. In Figure 2 membrane potential as a function of time during action potential is represented. Conduction of the action potential along the unmyelinated axons is based on the fact that depolarization opens also other Na^+ channels from nearby area. In myelinated axons, action potential can occur only in nodes of Ranvier, because the myelin sheath prevents ion transfer through the cell membrane. However, the current carried by Na^+ ions can easily flow inside the axon. When these ions reach next node of Ranvier, they depolarize the membrane so that Na^+ channels are opened, and a new

action potential is generated. This process is called saltatory conduction, and it's faster than continuous conduction in unmyelinated axons. Also thickness of the axon has an influence on conduction speed: the thicker the axon, the faster the conduction. Refractory period ensures that the signal doesn't turn backwards, but proceeds always in the same direction, in the case of motor neurons towards muscles. [2][4]

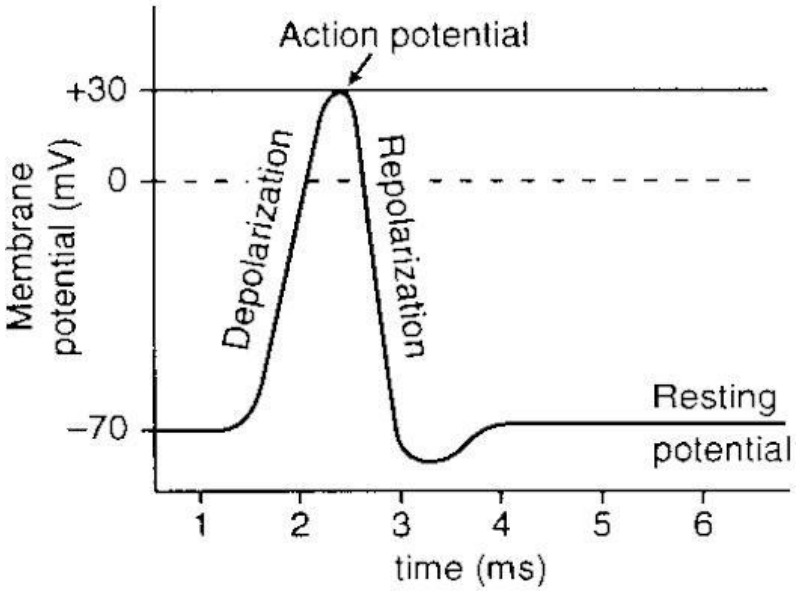

Figure 2. *Membrane potential as a function of time during an action potential. [19]*

Signal moves from between two neurons chemically. When an action potential reaches the presynaptic terminal of the axon, it opens Ca^{2+} channels which are located there. Concentration of Ca^{2+} is higher in extracellular than intracellular fluid, so Ca^{2+} flows inside the cell, allowing synaptic vesicles to secrete neurotransmitter to the synaptic cleft. In the somatic nervous system, the neurotransmitter between UMN and LMN is glutamate, and in the autonomic nervous system between preganglionic and postganglionic neuron acetylcholine (ACh). [2][4]

A neurotransmitter further diffuses to the postsynaptic terminal, where there are receptors to receive it. When enough receptors have been activated, Na^{+} channels are opened, allowing Na^{+} ions to flow in. Generated depolarized potential is the postsynaptic potential (PSP), more specifically the excitatory postsynaptic potential (EPSP), which can further generate action potentials in the postsynaptic dendrite. There are also inhibitory postsynaptic potentials (IPSP) in the nervous system. In the case of an IPSP, neurotransmitter makes postsynaptic membrane hyperpolarized, inhibiting the action potential generation. PSPs last much longer than action potentials. [2][4]

Between a neuron and a muscle, the mechanism is the same. The neurotransmitter in the somatic nervous system is ACh, and in the autonomic nervous system it is ACh or norepinephrine (also called noradrenaline). Also, the postsynaptic potential in the neuromuscular junction is called an end-plate potential (EPP). The EPP further generates an action potential in the muscle. The neuromuscular junction has been represented in Figure 3. [2][4]

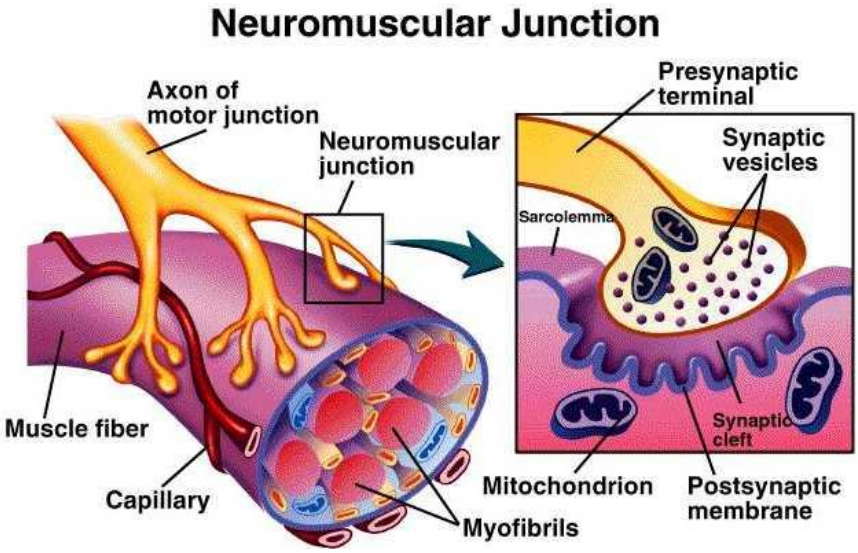

Figure 3. *Neuromuscular junction. [17]*

In the muscle fibers, action potentials proceed in same way as in neuron, even if rest membrane potential is usually more negative, about -90 mV. There are structures called T tubules in the cell membrane of skeletal muscle fibers, which conduct the action potential inside the fibers. Here action potential triggers the sarcoplasmic reticulum (SR), which is a structure on the surface of myofibrils, to open its Ca^{2+} channels and secrete Ca^{2+} ions. Binding sites for myosin on the surface of actin filaments are present, but they are normally covered by tropomyosin chains. Attached to tropomyosin are troponin molecules. Ca^{2+} ions bind to troponin, which causes the shape of tropomyosin to change, exposing binding sites of actin. Myosin now binds to these sites, initiating muscle contraction. When an action potential is completed, Ca^{2+} channels in the sarcoplasmic reticulum are closed. Since the SR also continuously pumps Ca^{2+} ions back inside, soon calcium is no longer attached to troponin. Then tropomyosin returns to its original shape, covering actin-myosin binding sites, and thus relaxing muscle. [2][4]

In cardiac muscle fibers the contracting mechanism is the same. However, even if autonomic motor neurons are used to adjust heart rate, pacemaker cells can generate action potentials independently. An action potential is also conducted to other cardiac muscle fibers via intercalated discs, so they don't require innervation of their own. In smooth muscle tissue, an action potential spreads via a diffuse junction to several muscle fibers at once, and can also spread from fiber to fiber via gap junctions. A contracting mechanism is different (details omitted here), but like in striated muscles, it's triggered by Ca^{2+} ions. There are no T tubules, but Ca^{2+} is obtained mainly from extracellular fluid, via Ca^{2+} channels opened by the action potential. [2][4]

When some skeletal muscle is used, the quantity of activated motor units, and also the action potential rate (APR) depends on the force required. There's also a difference between large and small muscles. In large muscles, the number of activated MUs and APR are low when force is low. When force is increased, more MUs are activated, until most of MUs in the muscle are in use. Only APR is increased noticeably after that. In small muscles, however, APR begins to increase earlier even if all motor units are not yet in use. When maximum force is produced, APR can be 50 Hz or higher. The refractory period sets the upper limit to APR. It's noticeable that with APRs higher than 20 Hz, muscle has no time to completely relax between APs. This is called a tetanized state. [3][31].

Another interesting phenomenon is that at a fixed force, APR is never fixed in muscles innervated by spinal nerves, but at intervals of two APs. However, in muscles innervated by cranial nerves APR can be fixed. This is due to the regulatory system of the spinal cord. [24]

2.2 Head area muscles and their innervation

Most muscles in the head area are responsible for facial expressions. All of them are innervated by the facial nerve (CN VII), which emerges from the brainstem between the pons and medulla, and divides to several branches (Figure 4). Even if a single muscle is often innervated by many branches, this can be generally divided into the following branches. [1]

The temporal branch innervates the frontalis, which wrinkles forehead skin and raises eyebrows, orbicularis oculi, which closes the eyelids, and corrugator supercilii, which draws eyebrows downward and medially and also produces wrinkles in frowning. [1]

The occipital branch innervates the occipitalis, which moves the scalp backward. Sometimes the frontalis and the occipitalis are considered parts (frontal and occipital bellies) of the same occipitofrontalis (or epicranius) muscle. [1]

The zygomatic branch innervates the zygomatic major, which draws the angle of the mouth backward and upward, and the zygomatic minor, which elevates the upper lip. [1]

The buccal branch innervates the following muscles. The procerus draws down the medial angle of the eyebrows and produces transverse wrinkles over the bridge of the nose. The nasalis consists of transverse and alar parts. The transverse part (compressor naris) draws the ala of the nose toward the septum and compresses the nostrils, and the alar part (dilator naris) opens the nostrils. The depressor septi nasi narrows the nostrils and draws the septum downward. The orbicularis oris compresses, contracts and protrudes the lips. The risorius retracts the angle of the mouth. The levator labii superioris elevates the upper lip and dilates the nares. The levator labii superioris alaeque nasi has three heads. The angular head elevates the upper lip and dilates the nostrils; the infra-orbital head raises the angle of mouth while the zygomatic head elevates the upper lip laterally. The levator anguli oris elevates the angle of mouth. The buccinator compresses the cheeks, expels air between the lips and aids in mastication. [1]

The marginal mandibular branch innervates the depressor anguli oris, which depresses the angle of mouth. The depressor labii inferioris depresses the lower lip and draws it lateralward. The mentalis raises and protrudes the lower lip. [1]

The cervical branch innervates the platysma, which is also important to muscles of facial expressions even though it extends to the thorax. Its function is to draw tight the skin of the neck. [1]

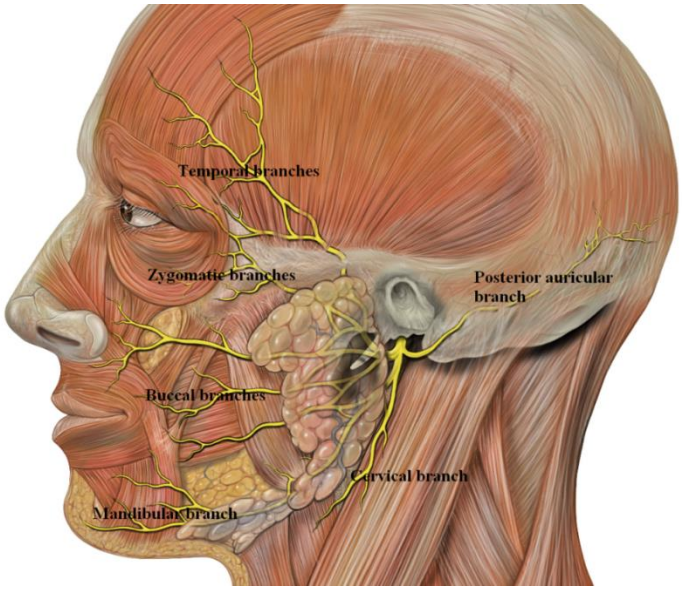

Figure 4. *Branches of the facial nerve. Modified from [18]*

Another large muscle group in the facial area is the mastication muscles. They are innervated by the mandibular nerve (CN V_3), which is branch of the trigeminal nerve (CN V). All four mastication muscles (temporalis, masseter, lateral pterygoid and medial pterygoid) move the mandible. In the Figure 5 the most important muscles of both facial expressions and mastication are shown. [1]

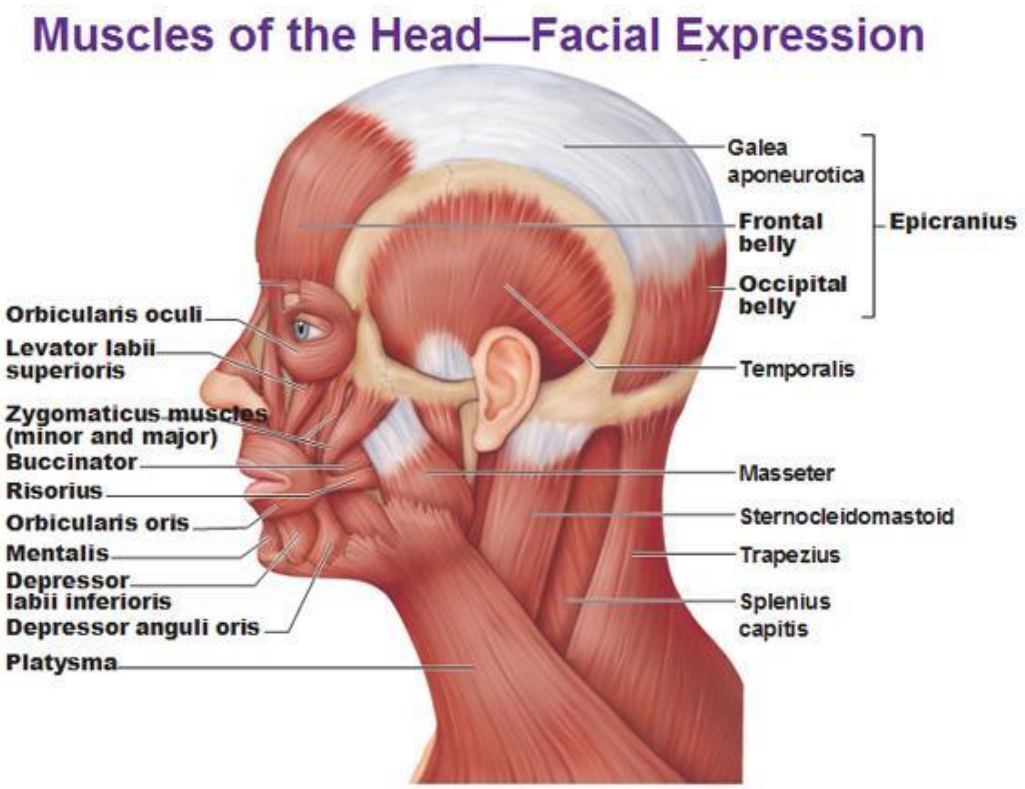

Figure 5. *Most important muscles in facial area. [21]*

Other muscle groups in the head area are following:

Intrinsic eye muscles dilate and constrict pupils and are responsible for focusing the eye. They are innervated by the oculomotor nerve (CN III) and sympathetic fibers from superior cervical ganglion (SCG), which is itself innervated by spinal nerves. [1]

Extra-ocular muscles move the eyeball and open the eyelids, and are innervated by the oculomotor nerve, trochlear nerve (CN IV) and abducens nerve (CN VI). [1]

External ear muscles move the pinna, whose significance is negligible in humans. They are innervated by the facial nerve (CN VII). [1]

The middle ear muscles are involuntary muscles which can move ossicles and thus dampen loud sounds. They are innervated by the facial nerve (CN VII) and the mandicular nerve (CN V_3). [1]

The intrinsic and extrinsic tongue muscles move the tongue, and are innervated by the hypoglossal nerve (CN XII). [1]

The palatal muscles are used mostly in swallowing. They are innervated by the mandibular nerve (CN V_3) and the pharyngeal branch of the vagus nerve (CN X). [1]

The pharyngeal, intrahyoid and suprahyoid muscles are used both in swallowing and speaking. The pharyngeal muscles are innervated by the glossopharyngeal nerve (CN IX) and the pharyngeal branch of the vagus nerve (CN X). The intrahyoid muscles are innervated by the ansa cervicalis, a nerve loop which is part of the cervical plexus (the plexus of the ventral rami of the cervical nerves C1-C4), and also directly by the first cervical nerve (C1). The suprahyoid muscles are innervated by the facial nerve (CN VII), the mylohyoid nerve (which is sub branch of the mandibular nerve (CN V_3)) and the first cervical nerve (C1). [1]

The laryngeal muscles move vocal folds during speaking, and are innervated by the superior and recurrent laryngeal nerves, which are branches of the vagus nerve (CN X). [1]

In the sternocleidomastoid of the neck, the splenius capitis, splenius cervicis and semispinalis, prevertebral and suboccipital muscles move the head. They are innervated by the cervical nerves, except for the sternocleidomastoid, which is innervated by the accessory nerve (CN XI). [1]

The erector spinae which extends back, and the trapezius and the levator scapulae which move the scapula, also extend to the neck. The erector spinae and levator scapulae are innervated by spinal nerves, but the trapezius is innervated by the accessory nerve (CN XI). [1]

2.3 EMG

Because tissues conduct electricity, the action potentials of muscles can be easily recorded. This is called electromyography (EMG), and the obtained signal is an electromyogram. An EMG can be recorded from the surface of the skin, which is considered a surface EMG (sEMG) or directly from muscle tissue. This is called a

needle EMG (nEMG). In needle EMG, better resolution is obtained, because there's no skin between muscle and electrodes to dampen the electric field. There are two types of needle electrodes. A monopolar (also called Morton's) needle requires another reference electrode. A concentric needle, instead, contains an inner core and an outer cannula, with the latter used as a reference. [4]

In needle EMG, action potentials of single muscle fibers can be distinguished in principle, but in surface EMG the smallest measurable signal is a sum of APs belonging to the same motor unit. This is called a motor unit action potential (MUAP). A signal where successive MUAPs of the same motor unit converge is called an MUAP train (MUAPT). Usually measured signal contains several MUAPTs (MUAPs of several motor units). [4] Figure 6 below represents approximately two seconds of typical needle EMG signal.

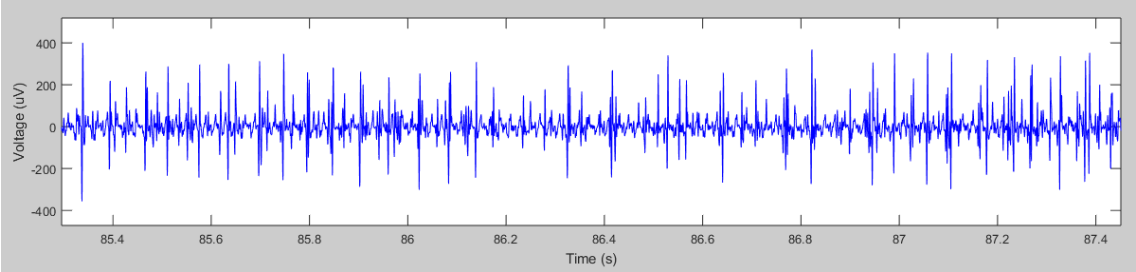

Figure 6. *Typical needle EMG signal.*

An EMG can in practice be recorded from all muscles. In this thesis, a facial EMG (fEMG) is recorded from frontalis, temporalis and masseter muscles. In real patients, fEMGs are often used to investigate emotional reactions. In this case, it often focuses on two muscles: corrugator supercilii, which is used in frowning, and zygomaticus major, which is used in smiling. [27]

Another common procedure in clinical neurophysiology is electroneuromyography (ENMG). It's divided into electroneurography (ENG), where motor neurons are electrically stimulated and conduction velocities are measured, and EMG, where the electric function of muscles is investigated. [4]

2.4 EEG

Tissue conductivity makes it possible to also record electric activity of the brain on the scalp. This is called electroencephalography (EEG), which is used to capture signal and

generate electroencephalograms. EEG signals originate mainly in the cerebral cortex. Unlike in an EMG, action potentials of the brain neurons are not seen in the EEG, because they are short-lived and temporally separate. Longer-lived postsynaptic potentials can be observed: however, PSPs of single neurons cannot be distinguished. The signal amplitude is usually some tens of microvolts. The first EEG (or, in fact, ECoG) was recorded for the first time on a human in 1924 by German neurologist Hans Berger, prior to which electric activity of the brain had been researched in animals. Earlier generations of EEG devices plotted the signal directly to paper, but nowadays data is converted digitally and processed with a computer. [4] Figure 7 below represents approximately 10 seconds of a typical EEG signal, recorded on a healthy, awake human test subject.

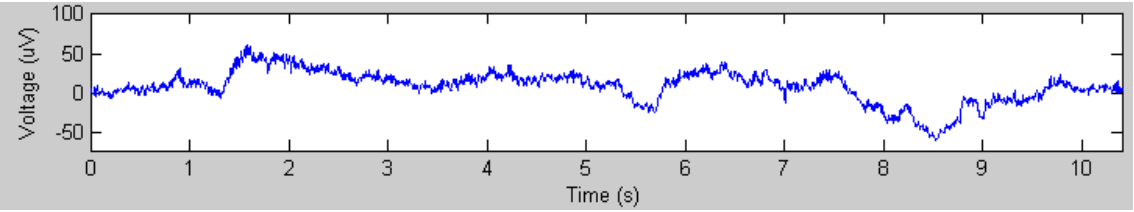

Figure 7. *Typical EEG signal, recorded from a healthy, awake human test subject.*

Usually 21 electrodes (channels) are used with a so called 10-20 system (Figure 8). In this system, the distance of nasion and inion, and the distance of frontal edges of the outer auditory canals are measured along the scalp. Electrode locations are then based on 10% and 20% percent values of these distances. In the naming of electrodes, Fp means frontopolar, F indicates frontal, T indicates temporal, C indicates central, P indicates parietal, O indicates occipital and A indicates auricle. Moreover, odd numbers refer to left hemisphere, while even numbers refer to the right hemisphere and z to the midline of the head. Common extra electrodes are zygomatic electrodes, which are set under the zygomatic arch. These allow for better signal acquisition from inferior part of the brain. If better resolution is needed, a 10-10 system where 75 electrode places have been defined can be employed. In research applications, the number of channels can be increased to 256 for example. Electrodes can be kept in place with a rubber net an electrode cap where electrodes are ready attached can be used. Skin dampens EEG signal significantly, because it has large impedance. Impedance can be reduced, however, by using electrode paste, and by removing stratum corneum by scratching the skin under electrodes. Shaving of the scalp at the location of electrodes is generally not needed. Impedances are usually measured before the EEG recording, the recommended maximum between electrode and reference electrode is 5 kΩ. [4]

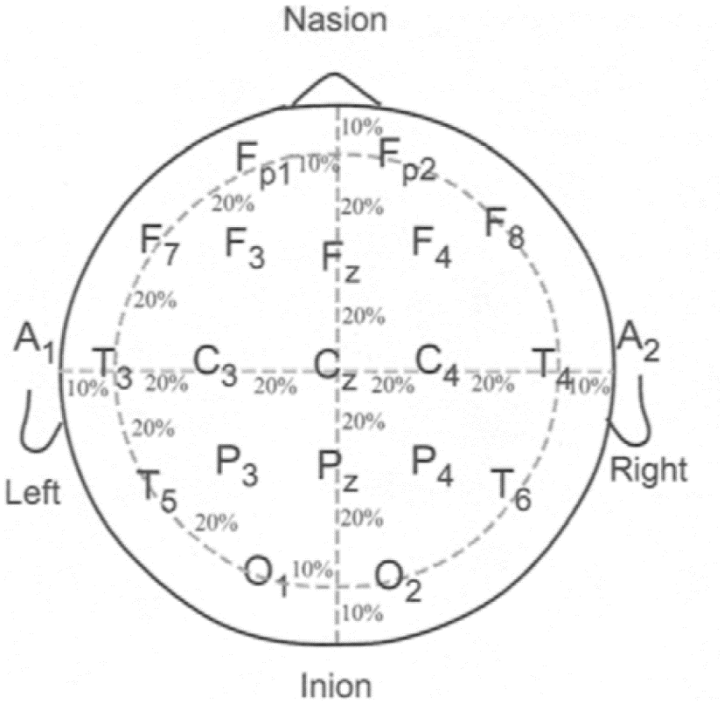

Figure 8. *Locations of the EEG electrodes in a 10-20 system. [3]*

In bipolar EEGs voltages are measured between two electrodes. In unipolar EEGs, voltages are measured between the electrode and some reference, which is often the average potential of all electrodes. During measurement using analog EEG devices, average potential was formed electrically by connecting electrode cables together. Nowadays a single physical reference electrode is generally used, and average potential is computed afterwards. This makes it possible to include only a portion of the electrodes in the average, if an interesting phenomenon is measured in the left hemisphere, the reference can be an average of electrodes in the right hemisphere. During EEG, electrocardiography (ECG) is usually recorded simultaneously. Standard 12-lead ECG can be used, but two leads in the patient's wrists or chest are often sufficient. Other common recordings during EEG are electrooculography (EOG) and respiratory airflow, which is obtained with a nose sensor. Video can also be recorded, which can be referenced afterwards to pinpoint moments when the patient moves his or her muscles. [4]

The most important application of EEG is diagnosing epilepsy. In that case, during the recording photic stimulation with strobe light, is often carried out to trigger epileptic changes in EEG. A hyperventilation test is also common, with which absence epilepsy can be diagnosed. Outside epilepsy diagnosis, EEG has been important in other applications such as diagnosing brain tumors, but developments in medical imaging methods has reduced its importance in this field. Often so called evoked potentials

(EPs) are also investigated, which are EEG responses to external visual or auditory stimuli. Sleep stages and structure can be seen from EEG, which makes it possible to also investigate different sleep disorders. During surgery EEG is used to monitor the depth of anesthesia. Brain death can also be easily found with EEG, which is flat in a brain dead patient. [4]

In normal EEG several frequencies are observed (mentioned boundaries are not exact and vary in source literature). Delta waves (< 4 Hz) are normally observed only during sleep. Theta waves (4 – 8 Hz) are observed mainly in children, but also in adults in dozing-off phase. Alpha waves (8 – 13 Hz) are observed when patient is awake with eyes closed. They originate in the visual cortex and are thus strongest in EEG in occipital area. Beta waves (> 13 Hz) are observed mainly when muscles are at rest. They originate in the motor cortex and are so strongest in EEG in frontocentral area. Gamma waves (> 40 Hz) are observed especially in conditions which require attention. [4]

During brain surgery EEG can be also measured directly from the surface of the brain. This is called electrocorticography (ECoG) and is usually used in epilepsy surgery. In some conditions, for example in locked-in syndrome where the patient can move only his or her eyes, electrodes can be implanted permanently under the skull, and thus construct a brain-computer interface. The advantage of ECoG compared to normal EEG is better resolution at high frequencies, because the skull dampens them more than lower frequencies. Electrodes can also be implanted on the top of skull, but under the scalp. The newest innovation is an EEG device with wireless subcutaneous electrodes; there are also wireless devices with normal surface electrodes. Wireless measurement is convenient especially in ambulatory EEG studies. [4]

2.5 EEG artefacts

There are many artefacts which can occur in EEG. This thesis concentrates on the EMG artefact, which occurs, if a patient moves or tenses muscles during the recording, especially in the head area. It becomes a problem especially in small children and patients unable to be still due to their condition. It’s usually impossible to completely eliminate EMG artefacts, because it’s located within the same frequency band as actual EEG (mostly at beta frequencies [25]). In proportion, if fEMG is recorded, EEG occurs as an artefact. However, this is usually is a smaller problem than EMG artefacts in EEG. [4]

EMG artefacts are naturally strongest when the source muscle (especially the activated motor unit) is directly under the electrode. So, in a 10-20 system artefacts in the frontopolar and frontal channels are mainly from the frontalis muscles, in the temporal

channels they come from the temporalis muscles, and in the occipital channels they come from the occipitalis muscles. If the zygomatic channels are used, the masseter muscles under the electrodes produce the strongest artefacts. Central and parietal electrodes are on the top of the galea aponeurotica where there are no muscles, so there are less EMG artefacts in those channels. However, an artefact can conduct to a more distant electrode, and that's a particular research problem in this Master's Thesis. [4]

If the eyes are moved during EEG recording, there are also EOG artefacts present, because the eye can be modelled by a large electric dipole. EOG artefacts are a problem especially in sleep EEGs during REM sleep. When the patient is awake, it can be restrained by recording the EEG with the eyes closed, which naturally eliminates also blinking EMG artefact (which is necessary if the recording of alpha waves is desired). Also, eye weights can be used on top of the closed eyes to further restrain eye movement. ECGs can also cause an artefact in EEGs, especially in patients with substantial neck musculature. The removal of EOG and ECG artefacts can be attempted afterwards with the help of the EOG and ECG signals recorded during the EEG. Also, recognition of the EOG artefact can be made easier by asking the patient to purposefully move eyes horizontally and vertically during EEG measurement. [4]

Motion artefacts arise when patient moves and causes the electrodes or electrode cables to move. They often occur simultaneously with EMG artefacts. Breathing doesn't cause a significant EMG artefact, because respiratory muscles are located far from the head, but especially deep breathing can cause a motion artefact by moving the head and electrode cables. The breathing artefact can be identified afterwards by measuring respiratory airflow during the EEG recording. Another extracorporeal artefact is a 50 Hz disturbance induced to the EEG device from the electrical network. Usually the 50 Hz artefact is simply filtered away. However, when the researcher is interested in the analysis of gamma waves which can occur in the 50 Hz range, the artefact can be prevented by recording the EEG in Faraday cage. In addition to the 50 Hz artefact, there are also higher harmonics at frequencies of 100 Hz, 150 Hz, etc., although weaker than the original artefact.

2.6 Basics of EEG and EMG signal processing

Analog EEG and EMG signals are nowadays converted to digital and processed with a computer. According to Nyquist's theorem, the sampling frequency of an A/D converter must be at least two times the largest frequency in the analog signal; otherwise aliasing of high frequencies occurs. Frequency of gamma waves can be up to 100 Hz, so usually a sampling frequency of at least 200 Hz is used. If needed, sampling frequency can be lowered by first filtering the analog signal with a low-pass filter. [5]

In the days of the old analog devices, the frequency spectrum was usually obtained with analog filter banks. Nowadays it's computed from a digital signal with the discrete Fourier transform (DFT):

$$\mathbf{X(n) = \sum_{k=0}^{N-1} x(k) w_N^{-kn}} \quad (1)$$

Where N is the length of the signal as samples, and w_N is N^{th} root of unity, which holds to the following:

$$\mathbf{w_N^N = (e^{2\pi i/N})^N = e^{2\pi i} = \cos(2\pi) + i\sin(2\pi) = 1} \quad (2)$$

Values of X(n) are usually complex, but with absolute values |X(n)| it's easy to see which frequencies the signal contains. Instead of Formula 1, DFT is usually computed with fast the Fourier transform (FFT) algorithm. [5]

When signal X(n) has been filtered or otherwise processed, it can be returned to the time domain with the inverse discrete Fourier transform (IDFT):

$$\mathbf{x(n) = \frac{1}{N} \sum_{k=0}^{N-1} X(k) w_N^{kn}}, \quad (3)$$

or in practice with the inverse fast Fourier transform (IFFT) algorithm. [5]

The basic operation in frequency domain is filtering. There are four filter types. A low-pass filter passes frequencies lower than a certain cutoff frequency, and filters the higher frequencies off. A high-pass filter works vice versa, so it passes high frequencies and filters off low frequencies. A band-pass filter passes the frequencies within a certain range, and a band-stop filter passes the frequencies outside a certain range. In practical filters (differing from ideal filter), amplification is never exactly one in a passband or exactly zero in a stopband, and there's a transition band between a passband and a stopband. [5]

All filter types are exploited in EEG and EMG signal processing. A high-pass filter is used to filter DC and low frequency components off, because they harm further processing of the signal. A low-pass filter is used to filter high, non-physiological frequencies off. Often both are needed, then it's worth it to use band-pass filter. Electricity's 50 Hz artefact is usually filtered away with a notch filter, which is a band-stop filter with a very narrow stopband. An EMG artefact cannot usually be filtered away from the actual EEG, however, because they occur in the same frequency band. [4]

In the days of analog devices analog filters were used. They are implemented by analog electronic components (in their basic forms: resistors, capacitors and inductors). Cutoff frequencies are determined by values of those components. The disadvantage in analog filters is that the properties of the components change when they age, and also vary with

temperature. Nowadays digital filters are used, which are implemented with a general-purpose computer or separate signal processor. In real-time signal processing, signal processors are often used because they are faster. [5]

Digital filters are represented with difference equations:

$$\mathbf{y(n) = \sum_{k=0}^{K} a_k x(n-k) + \sum_{m=1}^{M} b_m y(n-m)}, \quad (4)$$

where x(n) is the input signal and y(n) is the output signal. As seen from the equation, current output sample is calculated from the current input sample, some number K of previous input samples, and some number M of previous output samples. If there's no the latter sum term (current output sample doesn't depend on previous output samples), the equation becomes an FIR filter, and otherwise becomes an IIR filter. If x(n) = δ(n) (impulse), then y(n) is called an impulse response h(n). In an FIR filter there's a finite number and in an IIR filter there's an infinite number of h(n) terms deviating from zero. [5]

The properties of the filter depend on coefficients a_k and b_m. The results of filtering improve with the more coefficients are used, but this lengthens computation time. In an IIR filter fewer coefficients are needed than in an FIR filter, so if speed is important, use of an IIR filter is optimal. However, the advantage of an FIR filter is that all frequencies are equally delayed. [5]

With impulse response, the filter can also be represented in the form:

$$\mathbf{y(n) = x(n) * h(n) = \sum_{k=-\infty}^{\infty} h(k) x(n-k)}, \quad (5)$$

where asterisk indicates convolution. [5]

Also, if a Fourier transform is taken from both the input signal and the impulse response, filter can be represented simply:

$$\mathbf{Y(e^{i\omega}) = H(e^{i\omega})X(e^{i\omega})} \quad (6)$$

Here $H(e^{i\omega})$ is the frequency response. It's usually complex, and its magnitude can be termed amplitude response and phase angle phase response. [5]

When a FIR filter is designed, it's usually started from the desired frequency response. A perfect frequency response would require an infinite number of coefficients, so some window function must be used (not further discussed here). The simplest window function is the rectangular window; MATLAB, however, uses the Hamming window as default. [5]

2.7 EMG decomposition

If there are MUAPs of several motor units in the EMG signal, it's often useful to perform a decomposition: in other words, extract MUAPs of single motor units. Several algorithms for decomposition have been developed. Here the leader-follower algorithm is presented, which has been successfully applied in practical problems. [3]

First, the leader-follower algorithm assumes that the number of motor units is not known beforehand, which is often the situation. If the number of motor units is known, it's better to use some other algorithm. Second, it's assumed that MUAPs have already been recognized for example on the grounds of spikes in the signal. In other words, leader-following algorithms only clusters the MUAPs, and cannot answer whether or not there is an MUAP occurring at the same moment of time. Last, in the basic version of the algorithm all MUAPs must be temporally separate, MUAP overlapping (or superposition) cannot be overcome. [3]

In the algorithm, MUAPs can be represented simply by vectors containing their potential values as a function of time. Another possibility is to use some feature vector, which is shorter than the original MUAP vector. This shortens computation time. The feature vector can be formed for example with a Karhunen-Loève transform (not addressed here). [3]

First the MUAP in the signal is naturally located in the first cluster. The center and spread of the first cluster are initialized:

$$\boldsymbol{\mu_1 = p_1} \tag{7}$$

$$\boldsymbol{C_1 = \kappa I} \tag{8}$$

Here p_1 is a vector of the MUAP (original potential vector or feature vector), κ is a design parameter representing uncertainty and I is an identify matrix.

The second MUAP (vector p_2) can be located in the first cluster or the new cluster. The choice is made by calculating the MUAP's Mahalanobis distance to the first cluster.

$$\boldsymbol{d^2(p_2, \mu_1) = (p_2 - \mu_1)^T C_1^{-1}(p_2 - \mu_1)} \tag{9}$$

If the Mahalanobis distance is smaller than some threshold value η, the MUAP is located in first cluster, and the center and spread of this cluster are updated:

$$\boldsymbol{\mu_1 = (1-\alpha)\mu_1 + \alpha p_2} \tag{10}$$

$$\boldsymbol{C_1 = (1-\alpha)C_1 + \alpha(p_2-\mu_1)(p_2-\mu_1)^T} \tag{11}$$

Here α is again a design parameter describing the update rate. Otherwise, the new cluster is formed and its center and spread are initialized with Formulas 7 and 8.

The same process is then continued, until all MUAPs have been assigned to clusters. However, if there already exist two or more clusters, the Mahalanobis distance to all of them must be calculated, and the smallest one is chosen. This distance is then compared to threshold η to decide if the MUAP belongs to the cluster with that distance, or to a new cluster. [3]

2.8 EMG simulation

It's often useful to simulate the EMG signal. In this task the most difficult part is modeling the morphology of a single MUAP. In one possible model, used by Jung, Meklenburg and Patrick [26], the positive spike of the MUAP is formed by following:

FOR i=1 TO fiber_length

$$\mathbf{MUAP(i)} = \frac{\mathbf{1}}{\sqrt{\mathbf{distance^2} + \left(\frac{\mathbf{fiber\_length}}{\mathbf{2}} - \mathbf{i}\right)^{\mathbf{2}}}} \tag{12}$$

ENDFOR

Here *fiber_length* is length of the muscle fiber and *distance* is the distance between the muscle fiber and the recording electrode. The units for *fiber_length* and *distance* have been not specified. It's observed, however, that the smaller the distance, the larger the MUAP amplitude; and the larger the fiber length, the larger the spike width. The negative spike is formed with same formula with minus sign ahead. The final MUAP is obtained by combining positive and negative spikes and padding some zeros (Figure 9).

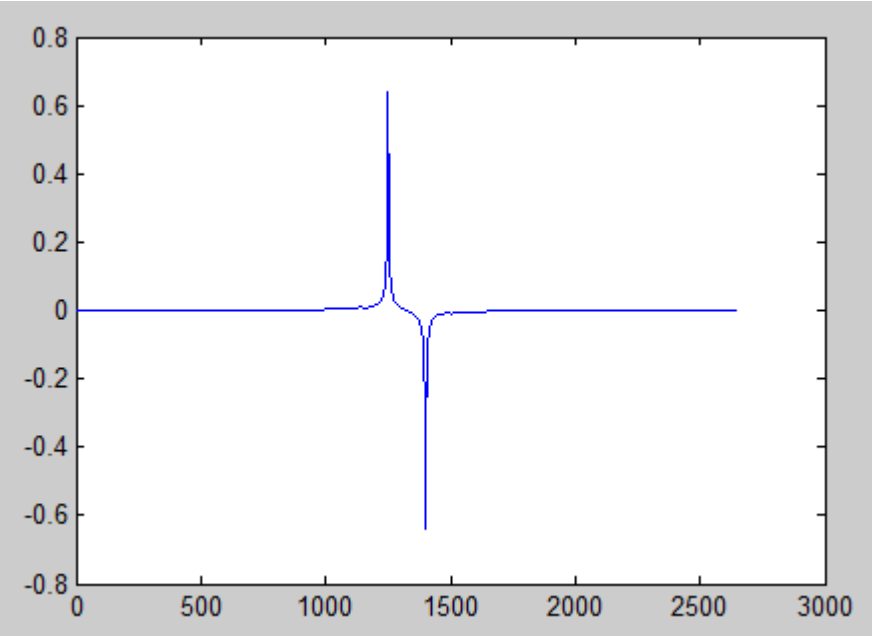

Figure 9. *Single simulated MUAP.*

Better, more physiologically based MUAP simulations have been developed (for example Hamilton-Wright and Stashuk [30]), but they are not discussed here in depth. The Validity of the simulation must be tested by comparing the simulated and the recorded MUAPs with some other method (in mentioned the study, for example, means and standard deviations of the samples has been compared).

Mathematically, the MUAP can be represented also as impulse response of a filter, h(t). In that case the MUAP intervals of a single motor unit can be represented by the sum of the impulse functions:

$$\mathbf{d_E(t)} = \sum_{k=1}^{M} \boldsymbol{\delta}(\mathbf{t} - \mathbf{t_k}) \qquad (13)$$

where t_k is time of kth MUAP. When simulating the EMG of facial muscles, the interval $t_k - t_{k-1}$ can be constant, in another case random values can be obtained by using a Gaussian distribution.

Now the EMG signal of single motor unit is obtained by:

$$\mathbf{u(t)} = \mathbf{d_E(t)} * \mathbf{h(t)} = \sum_{k=1}^{M} \mathbf{h}(\mathbf{t} - \mathbf{t_k}) \qquad (14)$$

Finally, total EMG signal is obtained by summing the signals of motor units.

$$\mathbf{x(t)} = \sum_{l=1}^{L} \mathbf{u_l}(\mathbf{t}) + \mathbf{v(t)} = \sum_{l=1}^{L} \sum_{k=1}^{M_l} \mathbf{h}\left(\mathbf{t} - \mathbf{t_{l,k}}\right) + \mathbf{v(t)} \qquad (15)$$

Here v(t) is the optional noise signal. [3]

2.9 Volume conductor modeling

In addition to signal processing techniques, the EMG can also be investigated with a volume conductor model. In volume conductor modeling, body tissues are represented as a mesh of resistors, where resistance values depend on the tissue. If permittivity (capacitive properties) and permeability (inductive properties) of tissues are of particular interest, capacitors and inductors can be added to this mesh, too. The EMG source can be modelled with one or more voltage or current sources (dipole). [9]

In the direct problem, the source is known. Thus, potentials in all nodes and currents in all wires connecting the nodes can be calculated. In the inverse problem, potentials in some nodes are known and the parameters for the source must be solved. The inverse problem is always more difficult than the direct problem and usually there's no unique solution. The inverse problem isn't investigated in this Master's Thesis. [9]

Due to the quantity of components, an analytical solution is usually impossible even in the case of a direct problem, and numerical methods must be used. Common methods are FDM (Finite Difference method) and the newer FEM (Finite Element Method), which are not discussed in depth here. However, it's important to mention that in the FDM method elements between nodes are always cubical, but in FEM method they can have any shape. Currently, a popular software for volume conductor modeling is COMSOL Multiphysics, which uses the FEM method and tetrahedral mesh (Figure 10). However, if a voxel image (obtained for example from MRI imaging) exists, constructing the FDM model is easier, because the voxel is suitable for the cubical FDM element. [9]

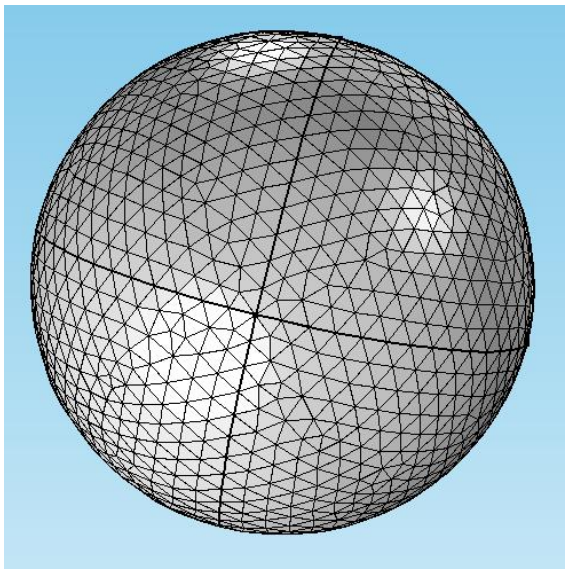

Figure 10. *Sphere constructed from tetrahedral FEM mesh in COMSOL Multiphysics. A resistor appears in every wire connecting the nodes.*

3. METHODS

The experimental work for this Master's Thesis was done at the Department of Clinical Neurophysiology at Seinäjoki Central Hospital. The human test subject was the author of the thesis himself. Using real patient data would have been possible, but it was decided that it was preferable to study the author instead to allow for simultaneous measurements (of EEGs and EMGs) and to avoid ethical approval for measurements.

3.1 Recordings

Several "exercise recordings" were taken, but only the data of the last recording was used in the computation (the exception being the needle EMG from the tibialis anterior, for which MUAP interval curve was plotted). In this last recording, EEG and facial EMG were recorded simultaneously with a sampling frequency of 2 kHz. The EEG was recorded with a standard 21-channel device (with extra zygomatic channels). Auricular channels linked together were used as a reference, and a separate ground electrode (Fpz) in the middle of the forehead was used. Loose button EEG electrodes were used. The reason for this was that when using the EEG electrode cap, electrodes can move on the scalp when facial muscles are moved. Also, it's difficult to insert the EMG needle into muscles through the cap. Afterwards it was noticed, however, that signals in the zygomatic channels were in practice found to be zero, so they couldn't be used in computations. It's probable that zygomatic electrodes were properly attached, but there was an error somewhere else in the system.

Facial EMG was recorded with the same EEG device with a concentric needle electrode. Morton's needle had been tested earlier, but it didn't work for simultaneous EEG and EMG recording. Amplitude differences of EEG and EMG signals were observed to be too large for the EEG amplifier, so a separate attenuator between the needle and the amplifier was used. The attenuation coefficient was not measured, however, which made it impossible to use absolute EMG signal values in calculations.

EMG was recorded from three facial muscles: frontalis (4 cm above midline of the eyebrow), temporalis (3 cm above the ear) and masseter (just below the zygomatic arch), both from the left and from the right side. These muscles (Figure 11) are relatively large and close to the scalp, so it can be assumed that they cause a significant portion of EMG artefacts in real patient EEG recordings. The frontalis is activated when the eyebrows are raised, and the temporalis and masseter are activated when the teeth

are clenched. Due to the zygomatic EEG electrodes being placed on top of the masseters, it's regrettable that signals from these electrodes were useless. EMG signals from the masseters were not omitted, however, because EMG artefacts from the masseters are also seen in standard EEG channels. During recording, the target muscle was tensed as lightly as possible, so that the minimum number of motor units would activate.

Also the ECG was recorded with two chest leads, along with respiratory airflow with the nose sensor, but these signals were not used in the computation. Video was recorded to make it possible to monitor afterwards what occurred at each moment of time. Recording duration was about 25 minutes. In Figure 12, the recorded EMG from the left temporalis is presented.

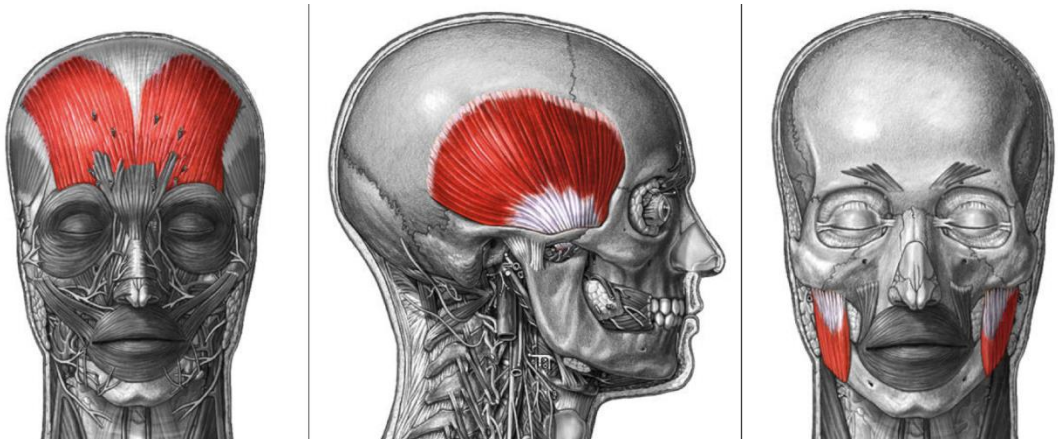

Figure 11. *Sketch of the frontalis, temporalis and masseter. [20]. The EMG was recorded from these muscles.*

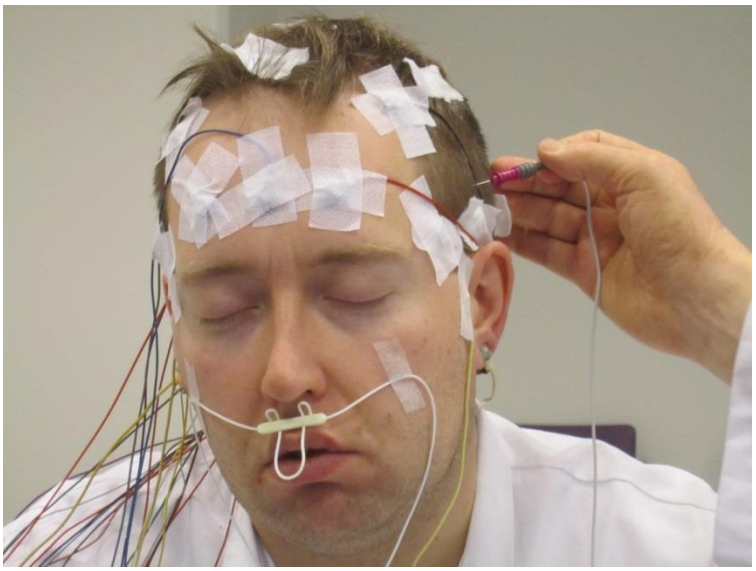

Figure 12. *Image from recording. The EEG is recorded with loose button electrodes attached to the head. The EMG is presently recorded with a needle from left temporalis. The nose sensor records respiratory airflow.*

Signals were recorded in .E-format (which was supported by Nicolet One software [10] used in the hospital), but were converted also to EDF (or actually EDF+) format. EDF (European Data Format) [12] is standard format for biophysical signals, and EDF+ [13] contains some new features, for example an annotation channel. In EDF format, signals were then read to MATLAB for processing. Also EDFbrowser [11] was used in investigating signals. It's a free software which contains part of same functionalities as commercial Nicolet One. Also, it's important to mention that ASCII format can also be used to store signals. However, if the number of channels is large, signals are long and sampling frequency is high, reading ASCII files in MATLAB is slow and consumes a large amount of computer memory, so it's better to use EDF format.

3.2 Processing of recorded signals

First the signals were investigated visually. A large DC or low frequency component was noticed in the signals, so they were first high-pass filtered. FIR filter with a Hamming window was used, and 2 Hz proved to be a good threshold frequency. Significantly lower thresholds left non-physiological components, and significantly higher thresholds began to distort the signal in the time domain. The same filter was used in both EMG and EEG channels. Signals were not low-pass filtered, because even reasonably high (200 Hz) thresholds seemed to distort signal. Testing different window

functions and adjusting the number of coefficients could have solved the problem, but that has been omitted. In the signal spectrum a 50 Hz artefact (and its higher harmonics) was also noticed, induced from electrical network, so signals were also filtered with a 50 Hz notch filter. This probably had no large significance, because the 50 Hz artefact was not clearly observable in the time domain. In Figure 13 an EMG signal after filtering can be seen.

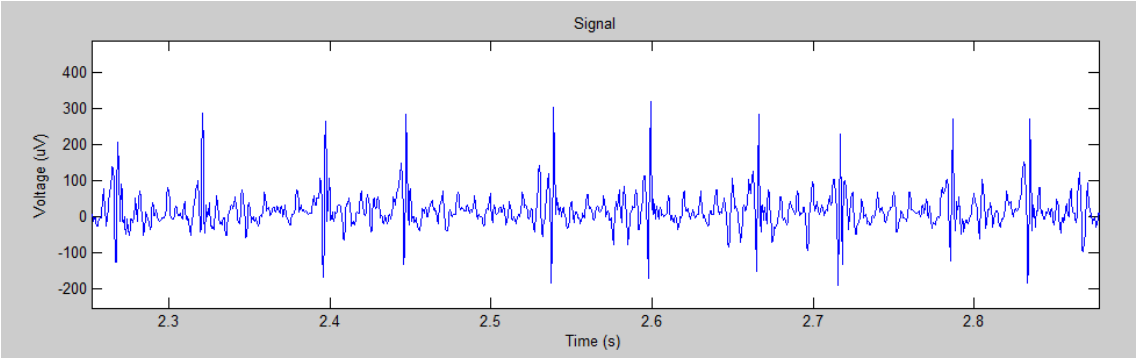

Figure 13. *High-pass filtered signal from EMG channel from the left temporalis. The MUAP of one motor unit is clearly seen.*

Recorded EEG signals were ear-referenced. Also average-referenced EEG signals were formed to cancel possible disturbances which occurred in auricular channels, and thus in all channels. In the average reference, the electrodes used were far from the EMG source. Moreover, the average reference differed for every electrode so that the electrode itself was not within the average. An example can be seen in Figure 14.

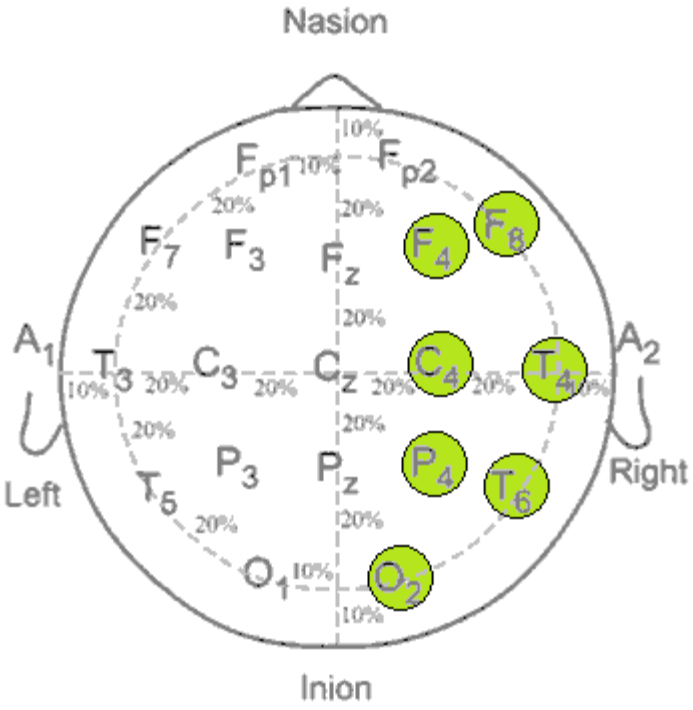

Figure 14. *Example, where the average reference is formed to electrode Fp2. The EMG source here is the left temporalis, so only electrodes on the right side of the head are included in the average. Electrode Fp2 itself is not included, however. Modified from [3].*

Even in the filtered EMG signal, disturbances with very large amplitudes were found, and also periods, where very many motor units were activated. So, a five second period which visually appeared to be the best option, was taken from each investigated muscle. From these five second periods were recognized spikes by demanding that amplitude in the spike exceeds some threshold value ($f(n) > N$), and moreover that the previous and subsequent signal values are smaller ($f(n-1) < f(n)$ and $f(n+1) < f(n)$). There are more complicated algorithms for spike recognition, but this simple method proved valid in this work. It's possible to obtain a more accurate temporal spike position for example by fitting a parabola to points $(n-1, f(n-1))$, $(n, f(n))$ and $(n+1, f(n+1))$ (Figure 15), in which case signal voltage values must also be interpolated. This proved unnecessary in this work, however, because of the reasonably large (2 kHz) sampling frequency.

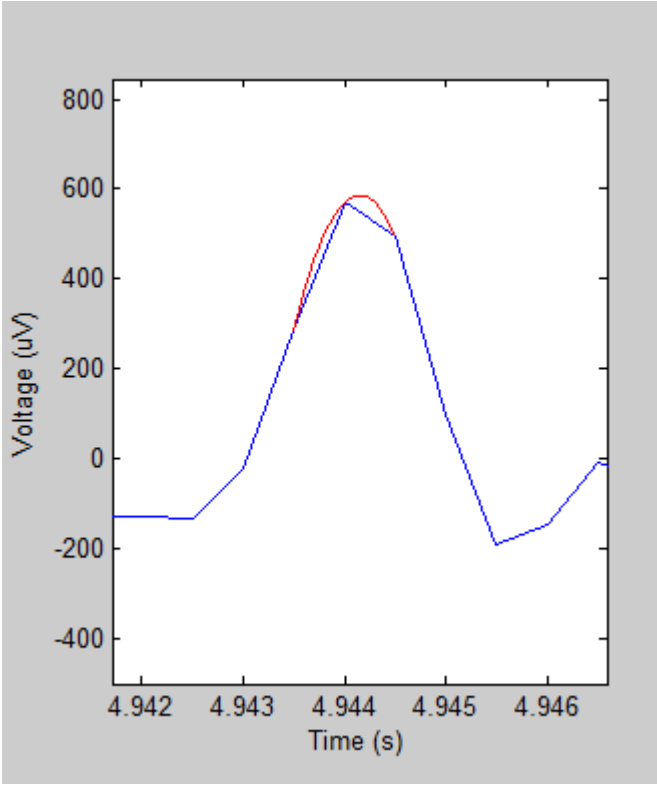

Figure 15. *Parabola fitted around a spike to obtain a more accurate temporal spike position. Not necessary with the 2 kHz sampling frequency, because maximum error is only 0,25 ms.*

It proved, however, that all recognized spikes didn't belong to MUAPs of the same motor unit. Since EMG signals from outside the measurement point should cancel, signal decomposition was further made by using EMGLAB (decomposition software implemented with MATLAB) [15]. In EMGLAB, it's possible to choose between two different algorithms, the default called simply automatic decomposition algorithm, and the second one called Montreal algorithm (both differing from the leader-follower algorithm represented in Chapter 2.7). Details of the algorithms are not covered here. Neither of the algorithms required any numerical design parameters, so using them was in a sense easier than using the leader-follower algorithm. It was decided to use default algorithm. User interface of EMGLAB is seen in Figure 16.

Only spikes belonging to one motor unit were left, others were removed. Choice of the motor unit was made on the grounds of MUAP amplitude (the larger, the better) and number of MUAPs of this motor unit (the more, the better). Errors in decomposition were possible. Since MUAP morphology can gradually change with time [3], it can be that MUAPs of the same motor unit were interpreted as MUAPs of different motor units. This was accepted to avoid other type of errors, namely interpreting MUAPs of different motor units as MUAPs of same motor unit.

Intervals of MUAPs belonging to same motor unit were calculated and interval curves were plotted. The corresponding interval curve was plotted also from the tibialis anterior, for which needle EMG had also been recorded. Information from MUAP intervals could be exploited in separating the EMG artefact from the measured EEG signal. Results have been represented in Chapter 4.1.

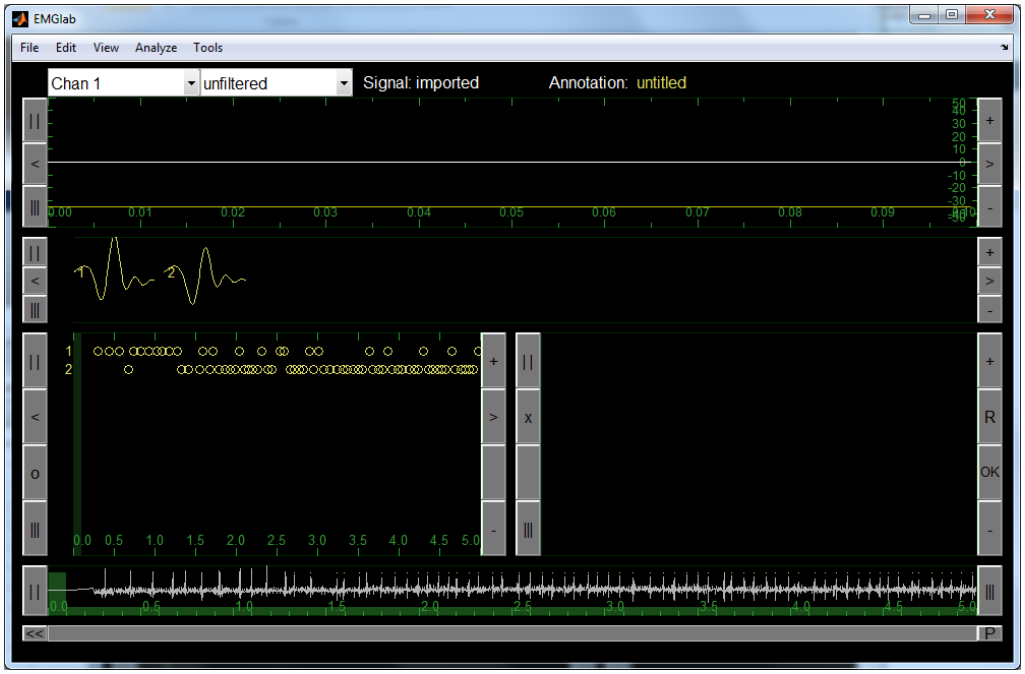

Figure 16. *EMGLAB decomposition software. MUAPs of two different motor units have been found from EMG signal from left temporalis.*

Next, 100 ms periods from the EMG signal around the spikes were taken and averaged. In averaged periods (Figure 17) disturbances vanish and only the pure MUAP signal remains. Averages were also taken separately from odd and even epochs, and they were then compared to each other (Figure 18). With this technique, it can be ensured that all MUAPs belong to same motor unit.

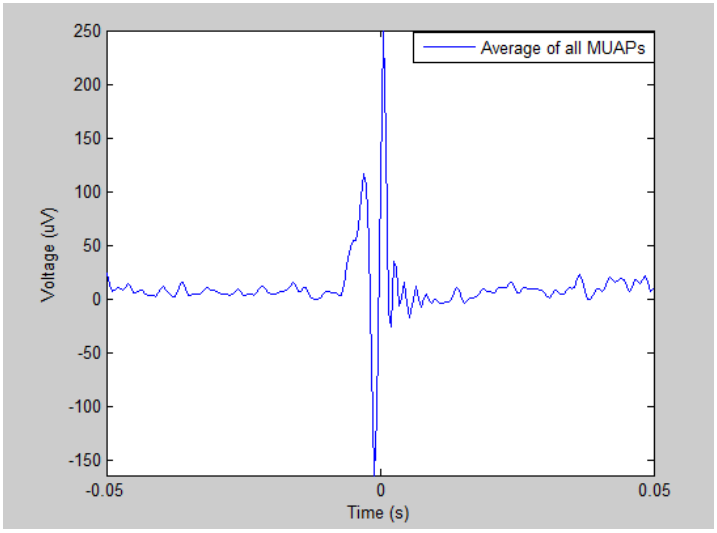

Figure 17. *100 ms averaged MUAP from the left temporalis.*

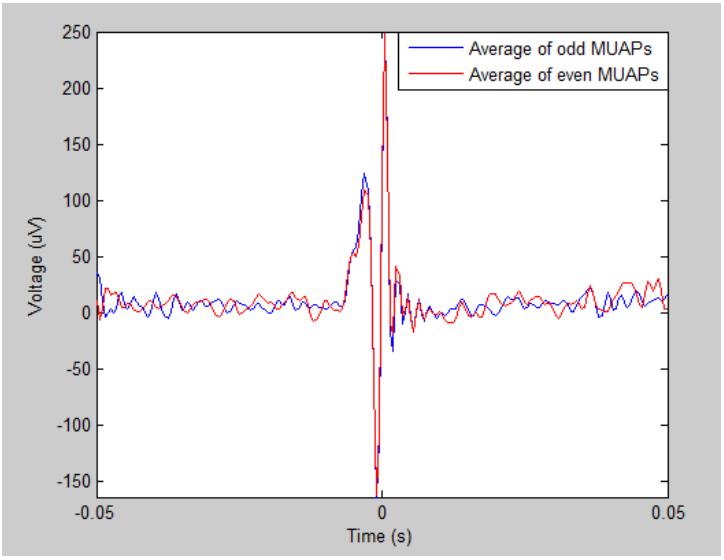

Figure 18. *Averaged odd and even MUAPs from the left temporalis. Because they are close to each other, they probably belong to the same motor unit.*

From the same positions as EMG measurements, periods were further recorded and averaged 100 ms from all EEG channels. In these averaged epochs, the actual EEG signal vanishes and the EMG signal conducted from muscle (EMG artefact) remains. Both ear-referenced and average-referenced EEG signals were used. Averaged EEG epochs were pre-investigated by plotting them to different images (Figure 19) and to the same image with the averaged MUAP from the EMG channel (Figure 20). The latter image is more easily visible (despite amplitude attenuations); phase delays between EMG and EEG channels are also visible.

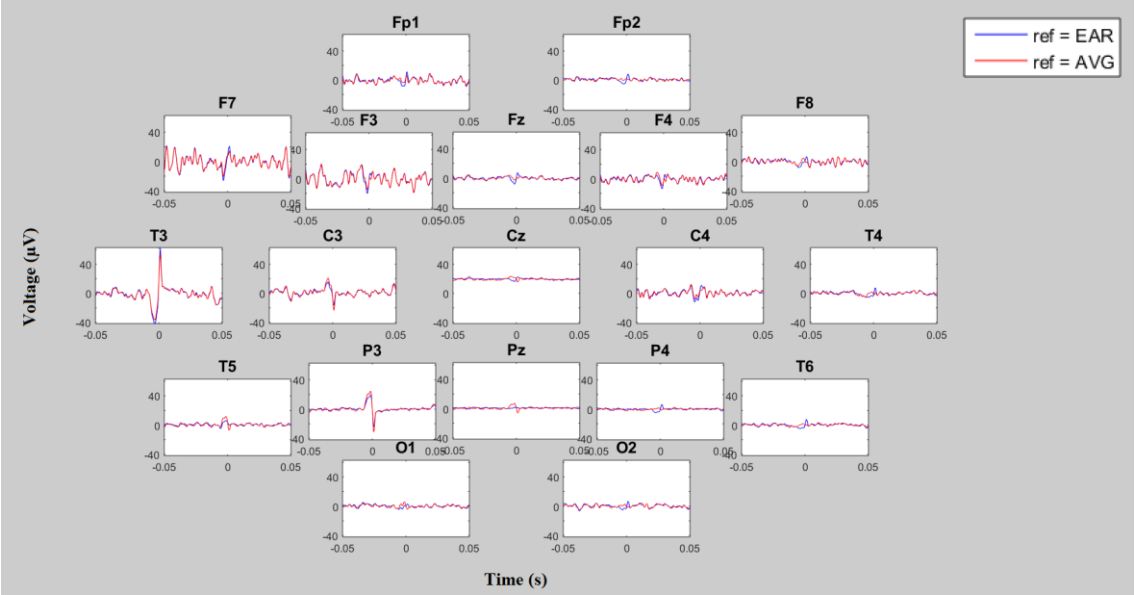

Figure 19. *100 ms averaged epochs from EEG channels. The EMG source here is the left temporalis*

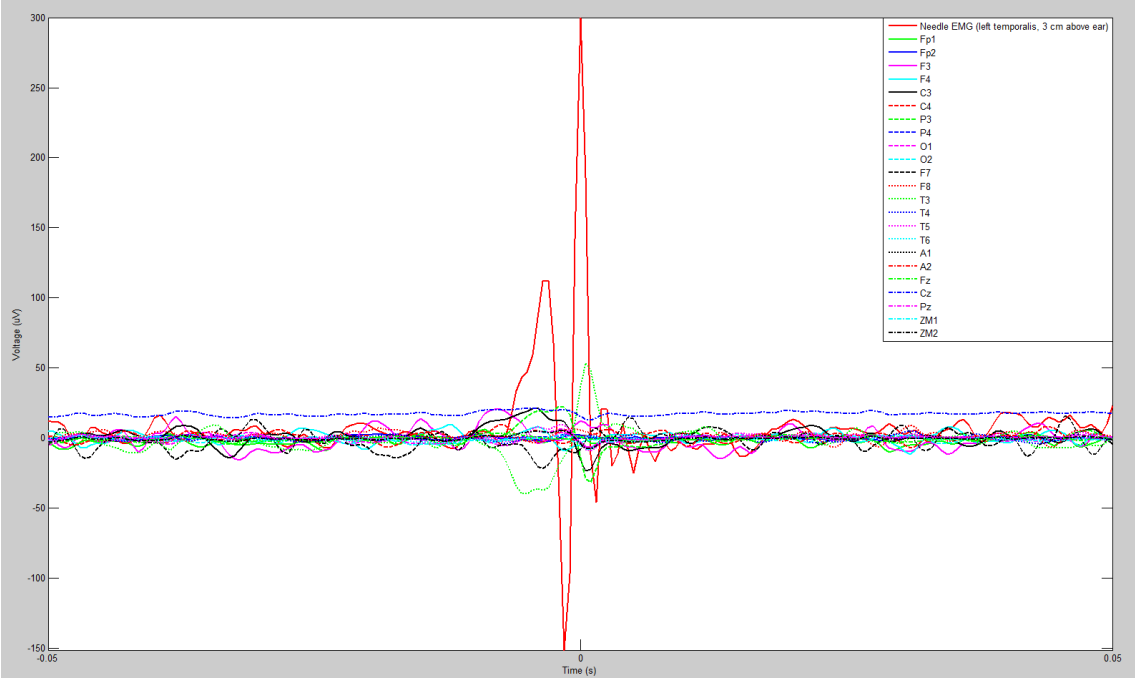

Figure 20. *100 ms averaged epochs from EMG and EEG channels in the same image. EMG source here is the left temporalis. Amplitude differences between EMG and EEG signals are not correct because of the unknown EMG attenuation coefficient.*

Distribution and dispersion of the EMG inside the head was illustrated also by plotting topographic maps. Single potential values needed here were obtained by taking peak-to-peak values from the averaged EEG channel epochs. Also here both ear-referenced and average-referenced EEG signals were used. Topographic maps were plotted with EEGLAB (software implemented with MATLAB) [14].

Since it's useful to know which EMG frequencies are most visible in EEG channels, and how much they are delayed, signals were further investigated in the frequency domain by considering tissues between EMG and EEG channels as a digital filter. Fourier transforms was taken from both input and output epochs and frequency response $H(e^{i\omega})$ was calculated with formula six. Amplitude and phase responses $|H(e^{i\omega})|$ and $\text{unwrap}(\arg(H(e^{i\omega})))$ were plotted. Here the MATLAB function *unwrap( )* plots a smooth curve where the phase angle can have any value. Without using it, the phase angle is always between -180º and 180º, and there can be discontinuities where the angle jumps from -180º to 180º or vice versa. Again, both ear-referenced and average-referenced EEG signals were used. Results have been represented in Section 4.3.

3.3 Simulation

If there's an interest in investigating how to separate the EMG artefact from measured EEG signal, EMG simulations are quite useful. In this Master's thesis, existing MATLAB code implemented by Jung, Meklenburg and Patrick [26] was employed. In this simulator the single MUAP has been modelled with Formula 12. Sampling frequency was set to 2 kHz (as in recordings).

The length of the muscle fiber has been included in the code. Facial muscle was approximated at 10 cm long with a conduction velocity of 3,5 m/s, thus length for samples is (0,1 m / 3,5 m/s) * 2000 ≈ 60. The value for conduction velocity was obtained and falls in the average range of 2 – 5 m/s, given by Sörnmo and Laguna [3].

Since the simulator was designed to simulate surface EMG, distance between the muscle fiber and the electrode was also randomized between the MUAPs of the same motor unit. Now the idea was to simulate a more accurate needle EMG, so distance was set as constant (exact value had no meaning, because the unit of distance was not specified). However, different distance values were used for different motor units.

In the original code, MUAP intervals of single motor unit were largely randomized. Randomizing was maintained even if it was utilized to simulate facial muscles tensed with constant force, but the range was set to a narrow range (50 - 70 ms), so the MUAP

frequency became 14,3 – 20 Hz. According to the interval curves obtained from the EMG recording, this is a realistic approximation.

Five motor units was used to describe the situation where muscle is tensed lightly (decomposition of recorded EMG signals also produced only a few motor units). For every motor unit, 100 MUAPs were generated. A segment of simulated signal is seen below in Figure 21.

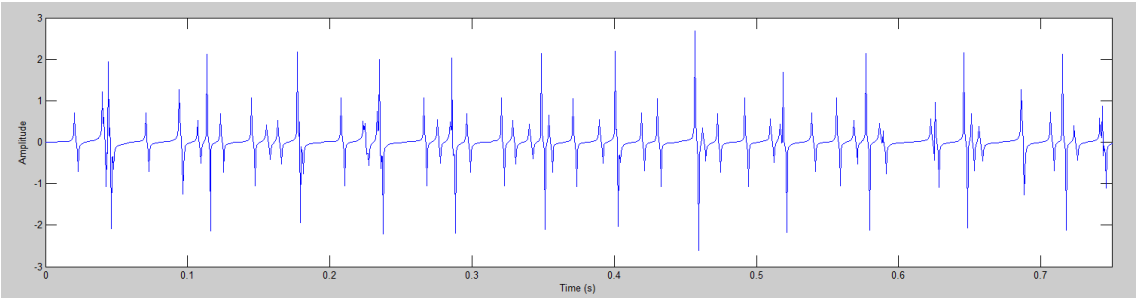

Figure 21. *Simulated facial needle EMG, when the muscle is tensed lightly.*

The Fourier transform was further taken from simulated signal. With the help of frequency responses $H(e^{i\omega})$ obtained from recordings, a simulated EMG artefact was applied to EEG channels with Formula six. Lastly, it was returned to the time domain with the inverse Fourier transform. Results have been presented in Chapter 4.4.

3.4 Volume conductor modeling

If the EMG artefacts in EEG channels are known, and there's a sufficiently good volume conductor model in use, it's possible to calculate the muscular origin of the artefact. In this Master's thesis the inverse problem was not addressed. Instead the quality of the model in the situation where EMG source is known was investigated, which is the direct problem.

A relatively simple head model was desired for this project. The simplest one is a homogenous sphere, but the ability to distinguish tissues was considered to be orderly. Thus, the model by Malmivuo and Plonsey [7] was chosen, represented in Figure 22. In this model the head has been divided into brain, skull and scalp tissues which have different resistances. Other values for tissue resistivity are found from other sources, so they are approximations. It's essential to set the model so that the skull has much higher resistivity than brain and scalp tissues.

The model was constructed with COMSOL Multiphysics (Figure 23). Alternative software would have been utilized, for example Noname Bioelectric Field Software (NBFS) implemented by Takano [16], which was used in earlier studies in the Department of Electronics and Communications Engineering [9]. Using NBFS proved difficult, however, so it was decided to employ COMSOL. NBFS uses the FDM method whereas COMSOL uses FEM. When the spherical model was used, it was easy to locate EEG electrodes on the scalp (their spherical coordinates are found e.g. from EEGLAB).

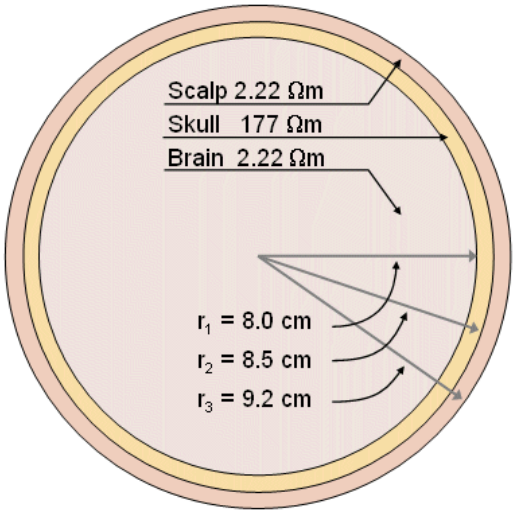

Figure 22. *Simple spherical head model. [7]*

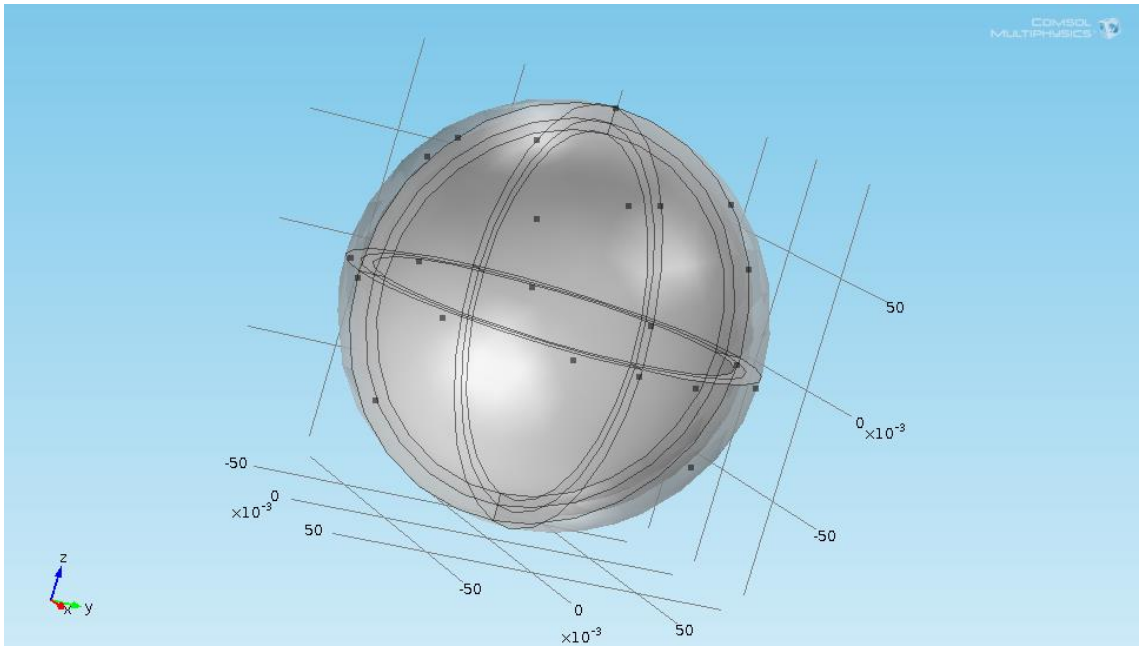

Figure 23. *Head model constructed with COMSOL Multiphysics.*

Even if the EMG signals were investigated, the muscle tissue itself was not modelled, because its resistivity is relatively close to scalp resistivity. If it had been added, it would have been worthwhile to take into account that there's no muscle tissue in the midline of the head. Other possibilities would have been adding eyes with their own resistivity value, and dividing the brain into white matter, grey matter and cerebrospinal fluid. Still another issue is tissue anisotropy. Muscle tissue is especially anisotropic, which means that it conducts electricity best in the direction of muscle fibers. Modeling anisotropic is difficult, however, so it's generally not carried out in volume conductor modeling.

In addition to resistivity, permittivity (capacitive properties) of tissues can also be taken into account. This was not included, so it was possible to use single potential values in the computation. When permittivity is used, temporal behavior of the signals must be taken into account. Permeability (inductive properties) of tissues was also omitted (they are not completely negligible, either, since the body contains ferromagnetic iron).

The most accurate head model would be a realistic model obtained from CT, MRI or cryosectional imaging data. In practice, the last method is the best. In cryosectional imaging of the head, the dead patient has been frozen and sliced (slice thickness can be in the hundreds of micrometers), and then each slice is photographed. Due to time consuming construction work and computation times, a realistic model was not used in this thesis. If it had been completed, perhaps an MRI image from test subject's head would have produced the best results. Ready raw data is available from The Visible Human Project [23] and other sources; an example of one slice of cryosectional data has been represented in Figure 24. Differences in head anatomy compared to the test subject's head could have influenced results, however. For example, if head imaging data belonged to a significantly overweight patient, who had substantial adipose tissue in the face. Also, using the FDM method (with NBFS or some other software) instead of FEM could have resulted in orderly results, if a realistic head model had been used. In that case voxels of the source image would have been suitable for cubical FDM elements.

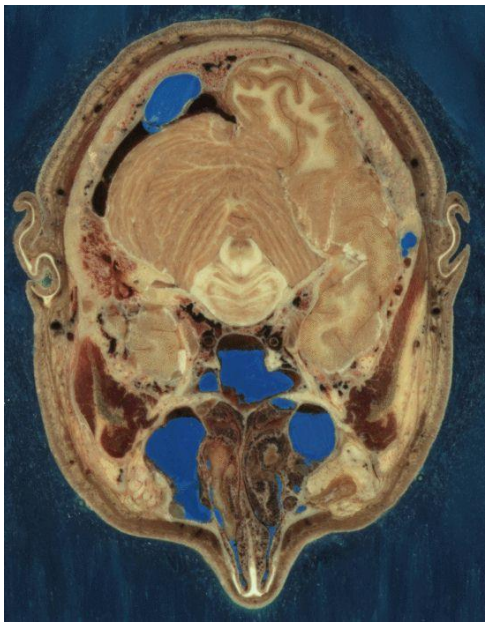

Figure 24. *One slice of cryosectional raw data from the Visible Human Project, suitable for constructing a realistic head model. Not utilized in this Master's Thesis. [23]*

The EMG source was modelled with a single voltage dipole for the needle. The distributed model, where the dipole has been distributed along a motor unit [28], is more accurate, but a simpler model was considered sufficient in this case. Also, instead of a voltage dipole, a current dipole [29] could have been used, but in this case both muscle resistivity and the motor unit cross-sectional area would have been known. A voltage dipole was chosen, because in this case the only quantity needed in the addition of potentials was conduction velocity.

Since the muscle tissue itself was not modelled, the needle was located in scalp tissue. In COMSOL, the voltage dipole was formed so that for two points different potential values were given, in this case the maximum and minimum of the averaged MUAP of the muscle in question. The distance between the points was obtained by multiplying the conduction velocity by the temporal distance between the MUAP maximum and minimum. The direction of the vector between these points was the direction of the muscle fiber. Dipole formation has been further clarified in Figure 25.

Conduction velocity could have been measured with two needles. Because only one needle was used, however, velocity was estimated to be 3,5 m/s. Its average in the range of 2 – 5 m/s was given by Sörnmo and Laguna [3], so this velocity is likely near the real value. The directions of the muscle fibers were roughly approximated. Dipoles of the frontalis and temporalis were set to point directly upwards (parallel to z-axis in Figure 26), even if it was known that in reality directions of muscles fibers also had some x- and y-components. Respectively, dipoles of masseters were set to point directly

downwards. If a realistic MRI-based head model had been in use, directions could have been looked at from an MRI image.

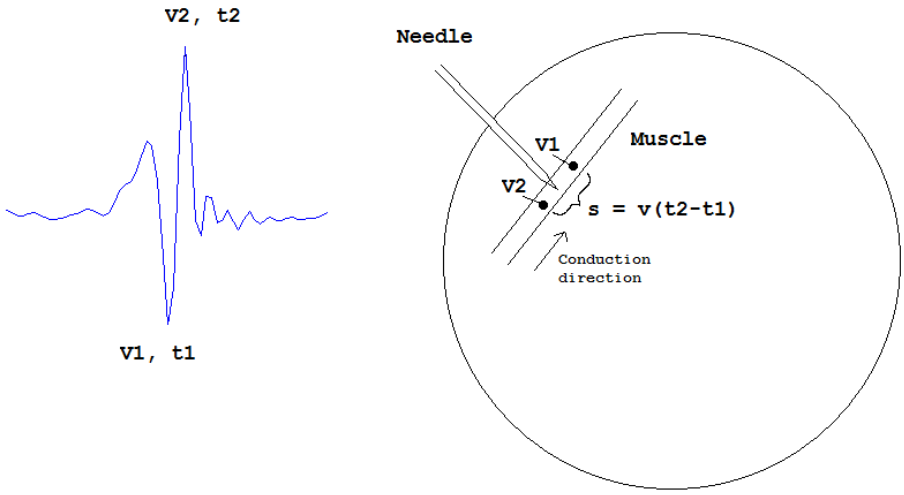

Figure 25. *Forming the voltage dipole for modeling the EMG source.*

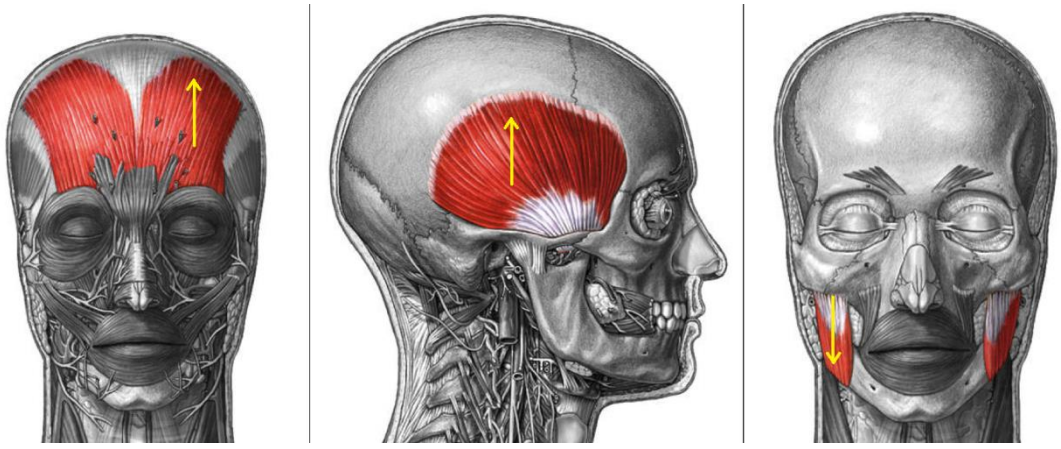

Figure 26. *Chosen dipole directions to frontalis, temporalis and masseter. Dipoles only have z components. If a realistic head model would had been used, the accurate direction could have been defined. Modified from [20].*

When the dipole was so defined, COMSOL calculated the potentials at all points on the surface of the head (Figure 27). After that, potentials in EEG electrode places were lowered, and the potential of the EEG reference electrode was subtracted from these

values (this, by the way, proved to be clumsy in COMSOL GUI, so the data was first exported to MATLAB). Here, the reference electrode was the ground point in the middle of the forehead (using ears as a reference would have required modeling the metal conductor linking them, too). Thus, peak-to-peak values of EMG artefacts in EEG channels were obtained. Topographic maps also were plotted. Computed results were compared to corresponding peak-to-peak values obtained from recording. Results have been presented in Chapter 4.2.

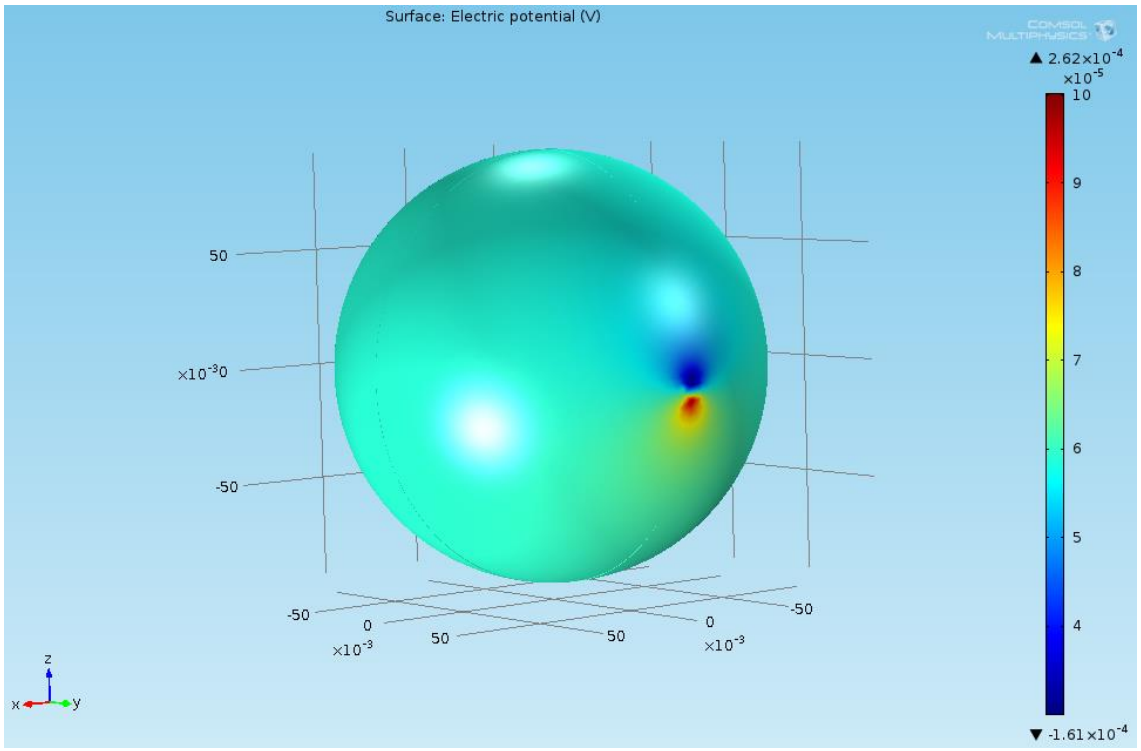

Figure 27. *COMSOL has computed potentials on the surface of the head, when the EMG source is the left temporalis. The potential gradient is largest near the source. The Face is in the direction of the positive x axis.*

4. RESULTS

4.1 MUAP intervals

Possible errors in EMG decomposition, more exactly interpreting MUAPs of the same motor unit as MUAPs of different motor units, make interval curves useless. Figure 28 only one piece of an interval curve (from left temporalis) is represented, where there should be no missing MUAPs in the intervals. Figure 29 features the interval curve from the tibialis anterior.

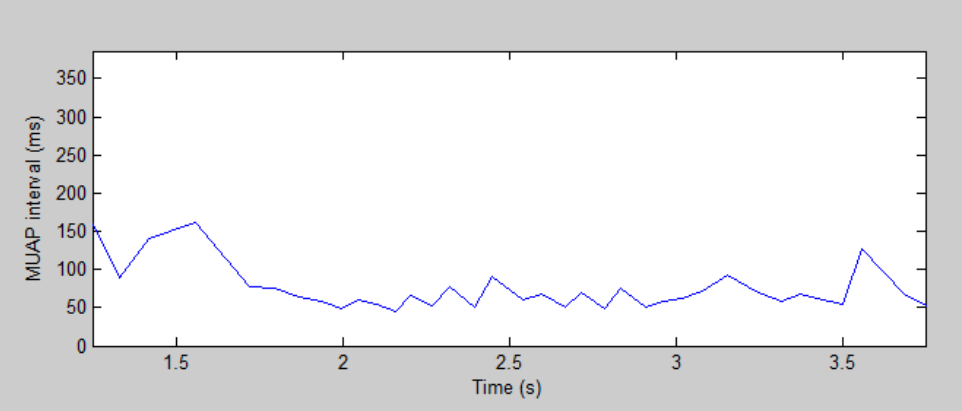

Figure 28. *MUAP interval curve from the left temporalis. Interval variation is reasonably small.*

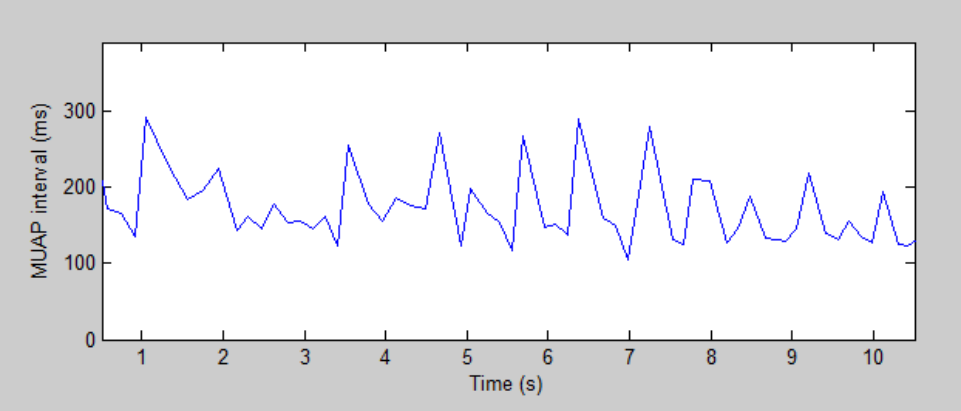

Figure 29. *MUAP interval curve from the tibialis anterior. Interval variation is reasonably large.*

4.2 Peak-to-peak values

In the first three tables peak-to-peak values of EMG artefacts in all EEG channels are represented, where the EMG source is one of six investigated muscles. Both values obtained from recording and values computed from the volume conductor model are shown. In recorded values, ear-referenced and average-referenced values are distinguished. Since the EMG attenuation coefficient was not measured, computed values are relative so that the numerical value in the channel nearest the EMG source is the same as the recorded average-referenced value. Measurement accuracy has been estimated to be ±0.1 µV. In Figures 30, 31 and 32 all tabulated values are also plotted to topographic maps.

	Left temporalis			**Right temporalis**		
Channel	**Recorded ear-referenced value (µV)**	**Recorded average-referenced value (µV)**	**Relative value computed from volume conductor model**	**Recorded ear-referenced value (µV)**	**Recorded average-referenced value (µV)**	**Relative value computed from volume conductor model**
Fp1	20.2	17.1	0.0	14.6	7.0	0.0
Fp2	13.6	6.5	0.0	19.6	18.1	0.0
F7	48.2	42.0	0.4	20.3	15.8	0.0
F3	38.8	40.1	2.0	19.6	17.9	0.4
Fz	15.8	9.0	0.9	7.4	13.4	1.1
F4	20.0	18.4	0.3	49.2	58.4	2.6
F8	15.1	15.6	0.0	61.6	52.1	0.5
T3	104.8	92.1	92.1	14.7	8.9	0.0
C3	32.1	45.0	4.8	10.0	8.5	0.5
Cz	6.6	8.0	1.2	3.1	11.8	1.6
C4	23.2	21.0	0.4	64.1	75.7	6.2
T4	13.1	9.8	0.0	127.4	125.4	125.4
T5	11.5	18.8	0.3	12.9	5.9	0.0
P3	43.1	56.0	2.1	8.6	5.3	0.4
Pz	2.3	13.2	0.9	3.8	10.0	1.1
P4	11.2	4.5	0.3	30.8	42.5	2.6
T6	12.8	6.8	0.0	13.2	17.2	0.4
O1	9.8	10.3	0.0	11.1	9.8	0.0
O2	13.1	9.5	0.0	11.6	10.3	0.0

Table 1. *Recorded and computed potential values from the left and right temporalis. Channels nearest the EMG source are grayed. It's clearly seen that the volume conductor model attenuates the signal too quickly when distance to source increases.*

	Left frontalis			Right frontalis		
Channel	**Recorded ear-referenced value (μV)**	**Recorded average-referenced value (μV)**	**Relative value computed from volume conductor model**	**Recorded ear-referenced value (μV)**	**Recorded average-referenced value (μV)**	**Relative value computed from volume conductor model**
Fp1	86.8	86.0	86.0	131.3	134.5	7.1
Fp2	82.6	82.8	7.2	77.4	81.2	81.2
F7	5.6	6.7	5.7	23.0	22.4	8.9
F3	29.4	30.1	28.0	71.3	75.7	12.3
Fz	9.8	14.6	20.3	25.4	29.9	20.0
F4	19.9	22.3	12.4	55.7	59.9	27.4
F8	9.8	10.2	9.0	43.3	44.2	5.5
T3	2.0	2.1	8.9	11.3	9.3	9.1
C3	3.5	4.6	12.6	9.2	12.8	10.5
Cz	1.0	1.6	12.4	4.6	9.0	12.2
C4	3.1	5.1	10.7	45.2	51.0	12.4
T4	3.2	3.6	9.2	29.0	30.4	8.7
T5	0.8	0.9	9.2	6.6	5.8	9.1
P3	1.1	1.7	10.1	3.3	5.9	9.7
Pz	2.2	3.4	10.2	1.7	3.7	10.1
P4	2.0	3.5	9.9	10.4	13.4	10.0
T6	0.7	0.4	9.3	5.6	4.9	9.1
O1	1.4	0.5	9.3	5.5	5.9	9.1
O2	2.6	2.3	9.3	6.7	5.6	9.1

Table 2. *Recorded and computed potential values from the left and right frontalis. Channels nearest the EMG source are grayed. Here the volume conductor model describes reasonably well how the signal attenuates when distance to source increases.*

	Left masseter			Right masseter		
Channel	**Recorded ear-referenced value (µV)**	**Recorded average-referenced value (µV)**	**Relative value computed from volume conductor model**	**Recorded ear-referenced value (µV)**	**Recorded average-referenced value (µV)**	**Relative value computed from volume conductor model**
Fp1	2.4	3.3	1.0	4.3	3.1	1.1
Fp2	5.2	4.1	0.4	12.3	12.1	2.6
F7	7.2	7.8	7.8	7.1	4.4	1.7
F3	10.0	11.8	2.3	4.3	3.8	0.2
Fz	1.6	2.8	0.7	6.9	8.3	1.8
F4	2.7	3.4	0.1	32.4	33.2	6.1
F8	9.9	9.5	0.7	23.1	20.4	20.4
T3	6.8	5.5	10.7	8.2	6.4	1.9
C3	6.7	9.4	2.3	2.9	4.3	0.4
Cz	0.3	3.0	0.5	2.3	4.7	1.4
C4	0.9	1.9	0.1	28.8	29.3	6.0
T4	6.3	6.9	0.7	26.8	24.1	27.8
T5	2.5	2.0	1.9	5.9	4.4	1.9
P3	1.1	1.9	1.0	3.6	3.7	0.6
Pz	0.8	1.3	0.2	2.1	1.8	0.6
P4	1.2	2.3	0.2	8.7	12.0	2.6
T6	2.5	2.3	0.7	7.5	5.5	4.8
O1	4.4	3.6	0.3	5.7	3.8	1.7
O2	4.6	3.6	0.6	6.6	5.3	0.7

Table 3. *Recorded and computed potential values from the left and right masseter. Channels nearest the EMG source are grayed. Here the volume conductor model describes reasonably well how the signal attenuates when distance to source increases.*

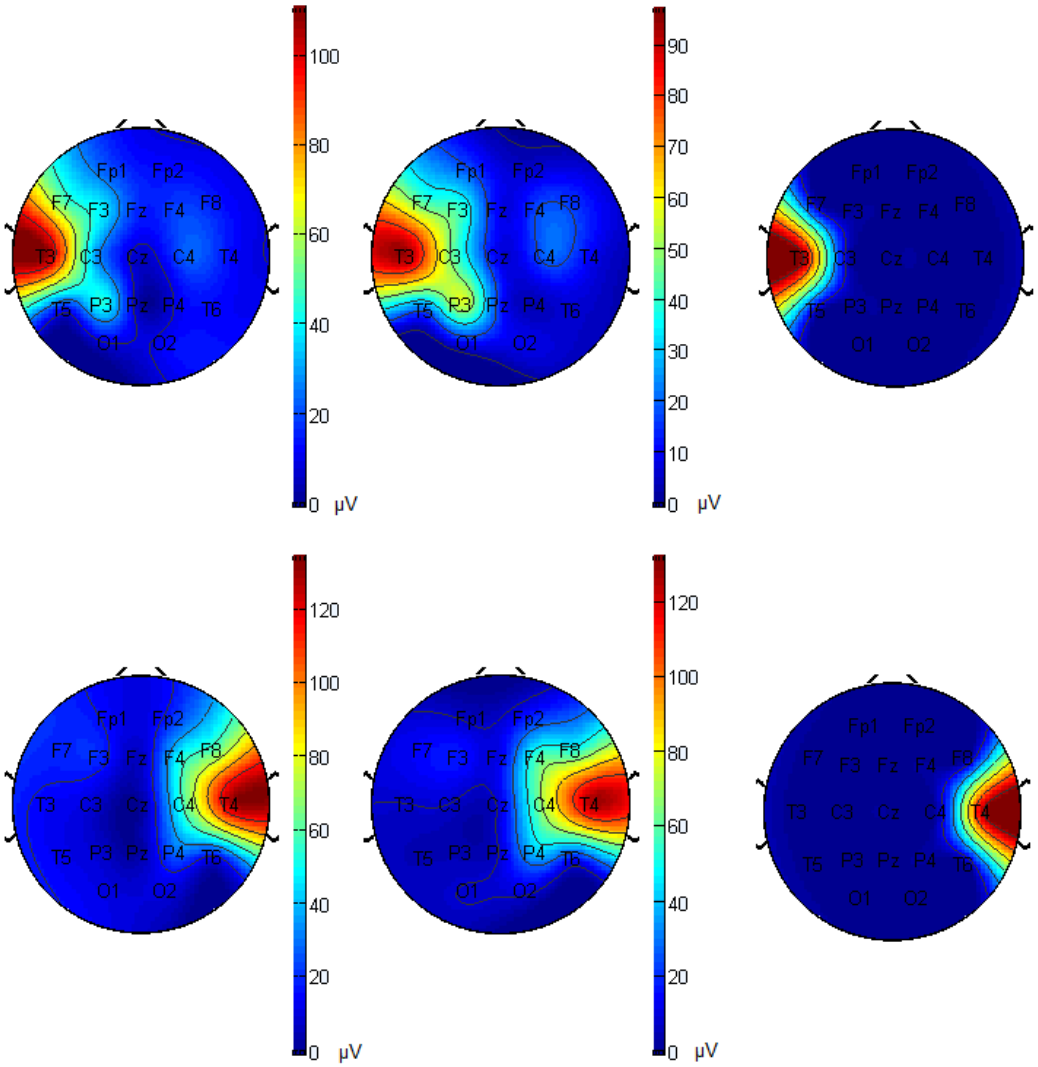

Figure 30. *Spreading of the EMG artefact of the left temporalis (above) and right temporalis (below). On the left ear-referenced values are used and in the middle average-referenced values obtained from recording are used. On the right relative values computed from volume conductor model are used. It's clearly seen that the volume conductor model attenuates the signal too quickly when distance to source increases.*

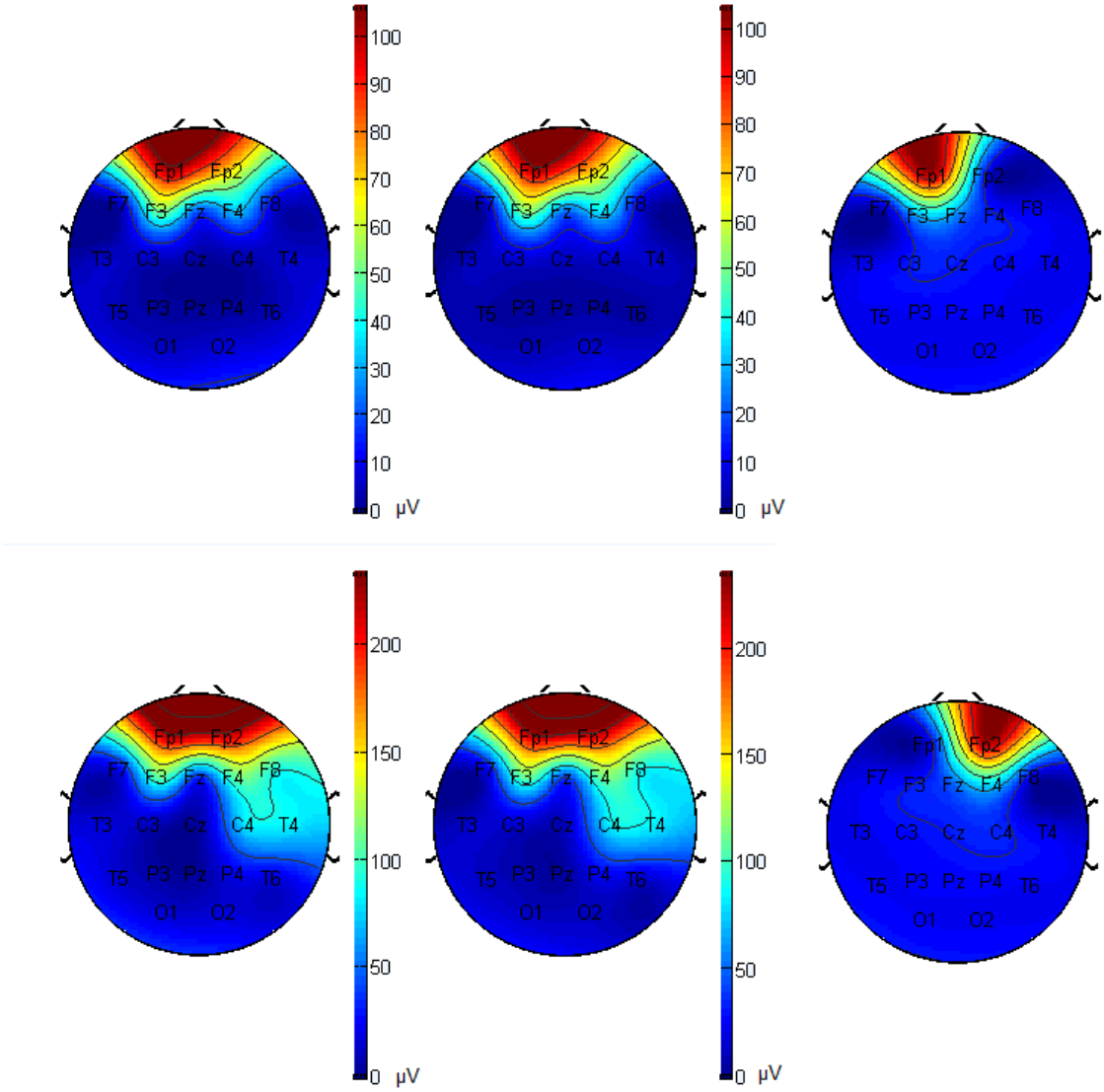

Figure 31. *Spreading of EMG artefact of the left temporalis (above) and right temporalis (below). On the left ear-referenced values are used and in the middle average-referenced values obtained from recording are used. On the right relative values computed from volume conductor model are used. Here the volume conductor model describes reasonably well how signal attenuates when distance to source increases.*

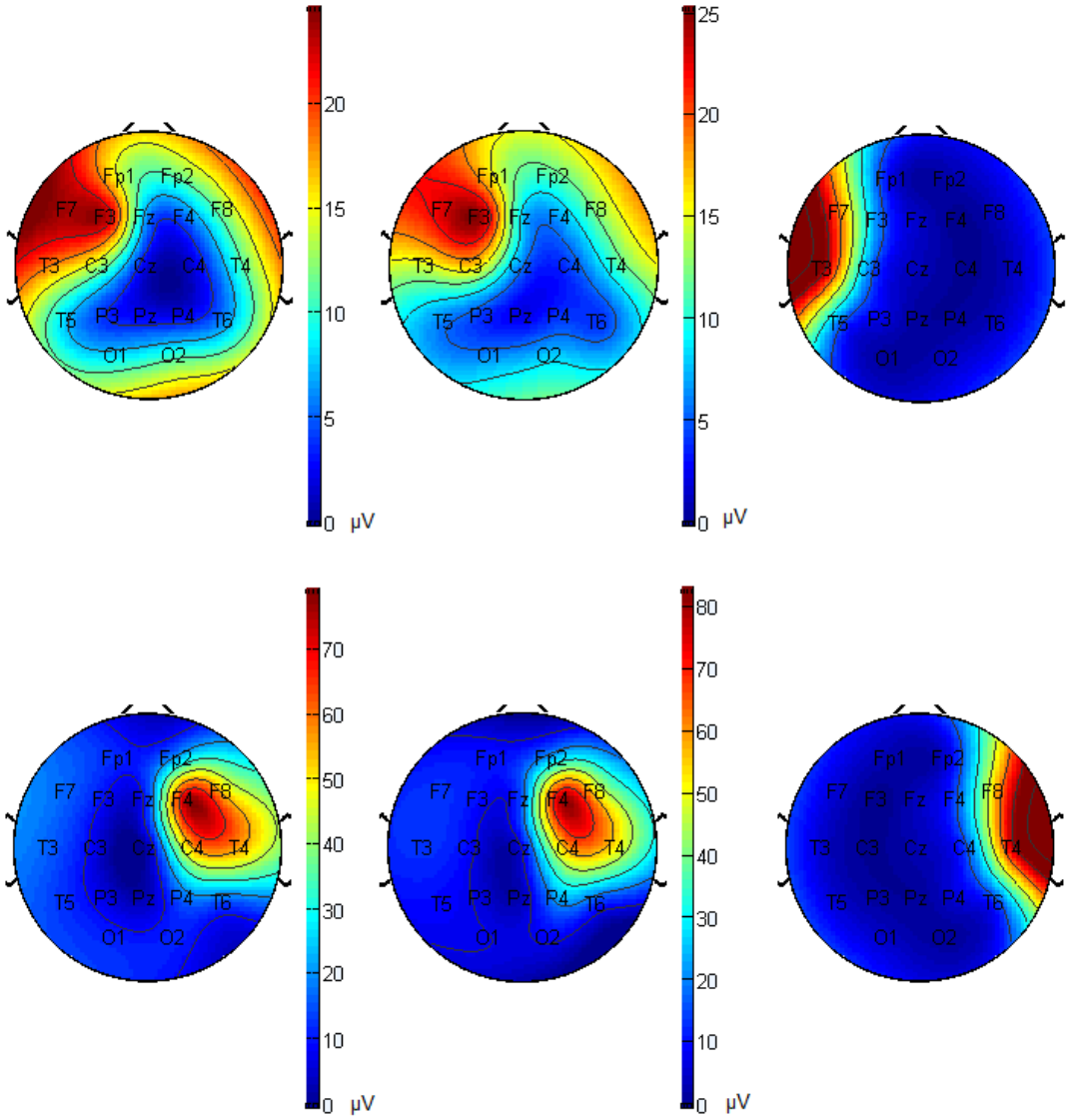

Figure 32. *Spreading of EMG artefact of the left masseter (above) and right masseter (below). On the left ear-referenced values are used and in the middle average-referenced values obtained from recording are used. On the right relative values computed from volume conductor model are used. Here the volume conductor model describes reasonably well how signal attenuates when distance to source increases. Some disturbance signal is seen in the left masseter's recording. It also misrepresents that signals from the zygomatic channels are now not in use.*

4.3 Frequency responses

In Figures 33-38 amplitude and phase responses of all six investigated muscles have been plotted, when tissues between the muscle and the EEG channels have been considered a digital filter. Blue curves correspond to ear-referenced values, and red curves correspond to average-referenced EEG signals. Amplitude responses have been

normalized for maximum amplification; when all channels are taken into account it is one. Absolute amplifications cannot be defined, because the EMG attenuation coefficient was not measured.

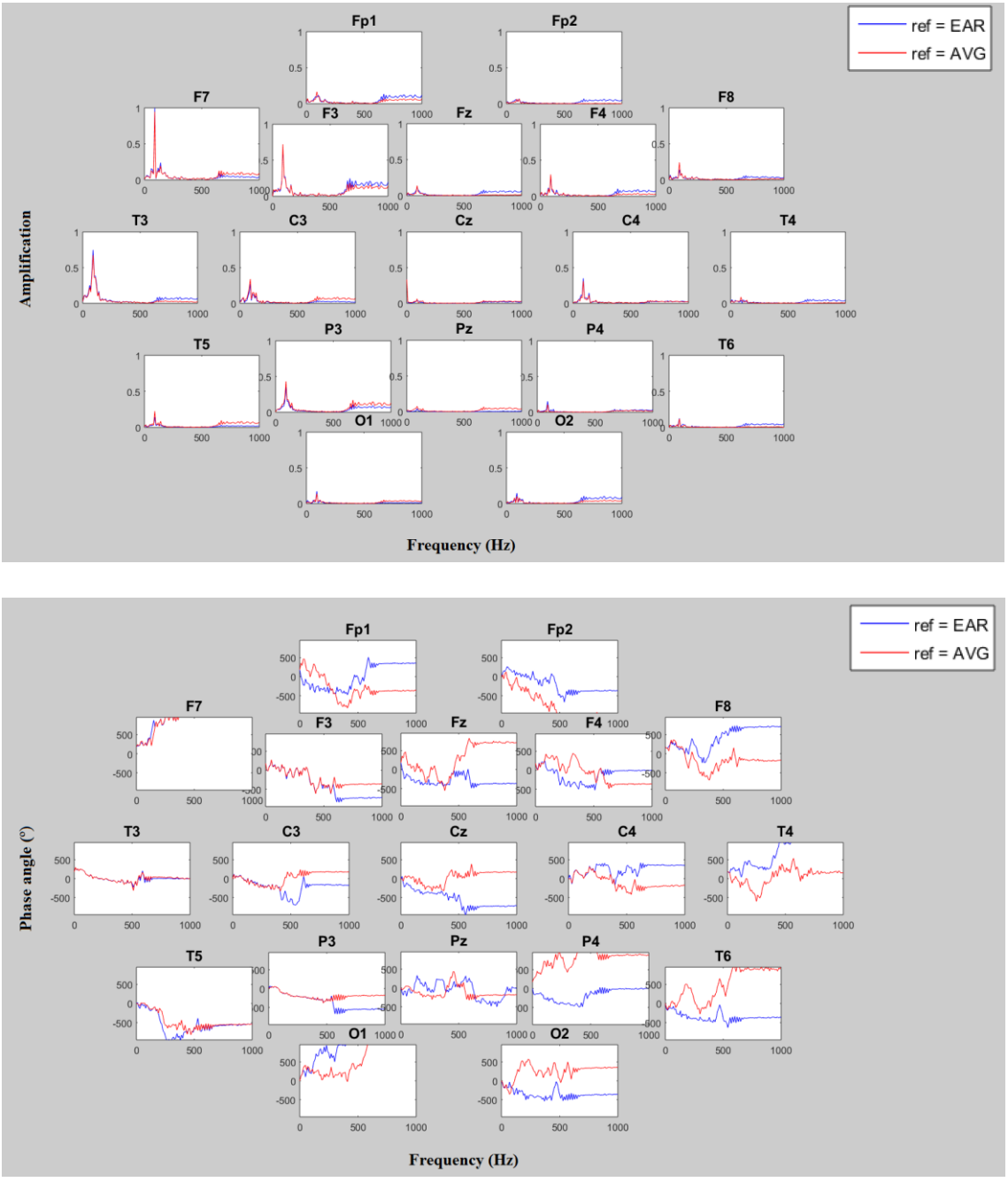

Figure 33. *Normalized amplitude responses and phase responses, when tissues between the left temporalis and the EEG channels have been considered a digital filter. It's clearly seen that the signal attenuates least in some frequency < 100 Hz. Large amplitude responses in frequencies > 500 Hz are non-physiological and occur due to pre-filtering. It's difficult to make conclusions from the phase responses.*

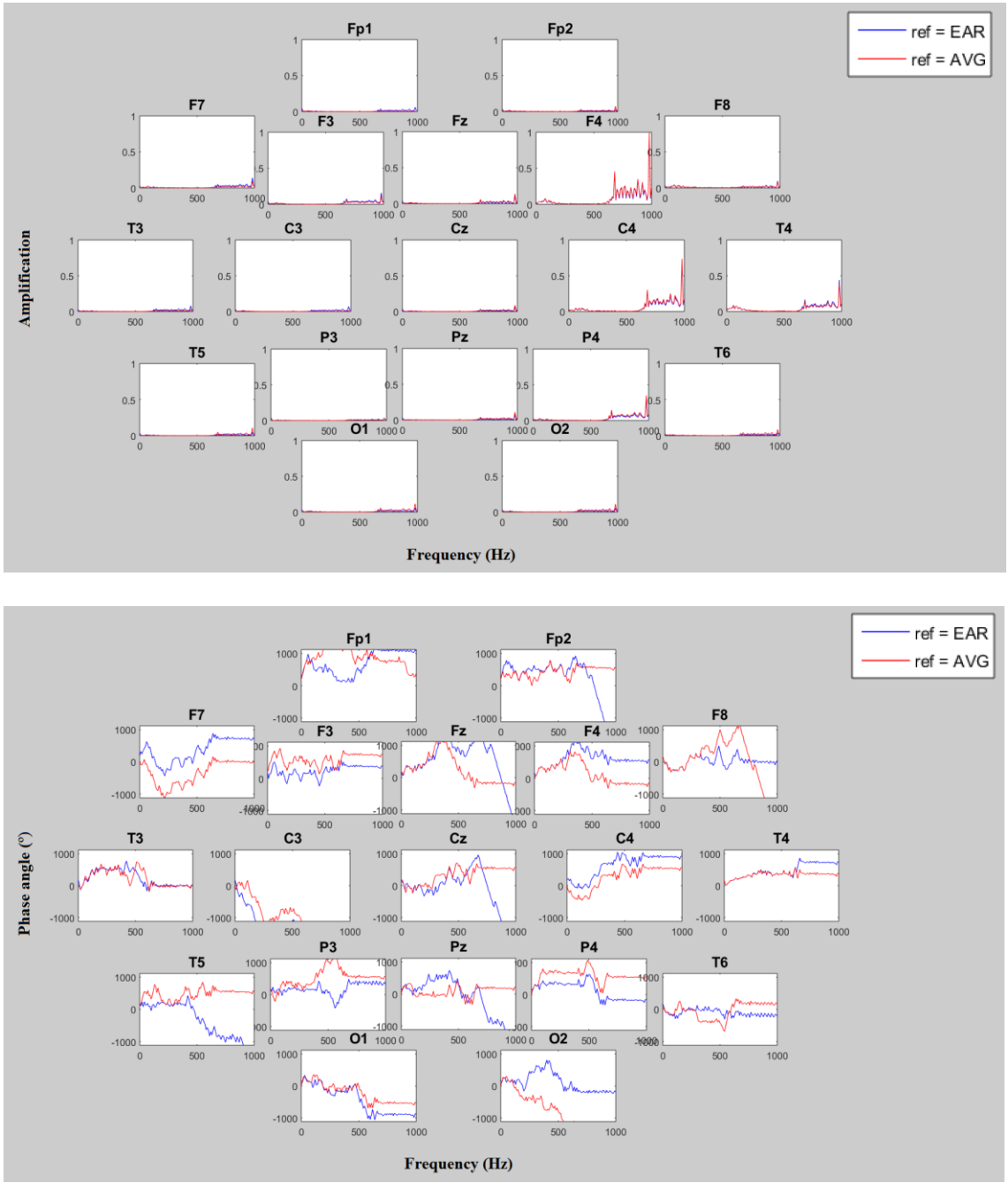

Figure 34. *Normalized amplitude responses and phase responses, when tissues between the right temporalis and the EEG channels have been considered a digital filter. It's clearly seen that the signal attenuates least in some frequency < 100 Hz. Large amplitude responses in frequencies > 500 Hz are non-physiological and occur due to pre-filtering. It's difficult to make conclusions from the phase responses.*

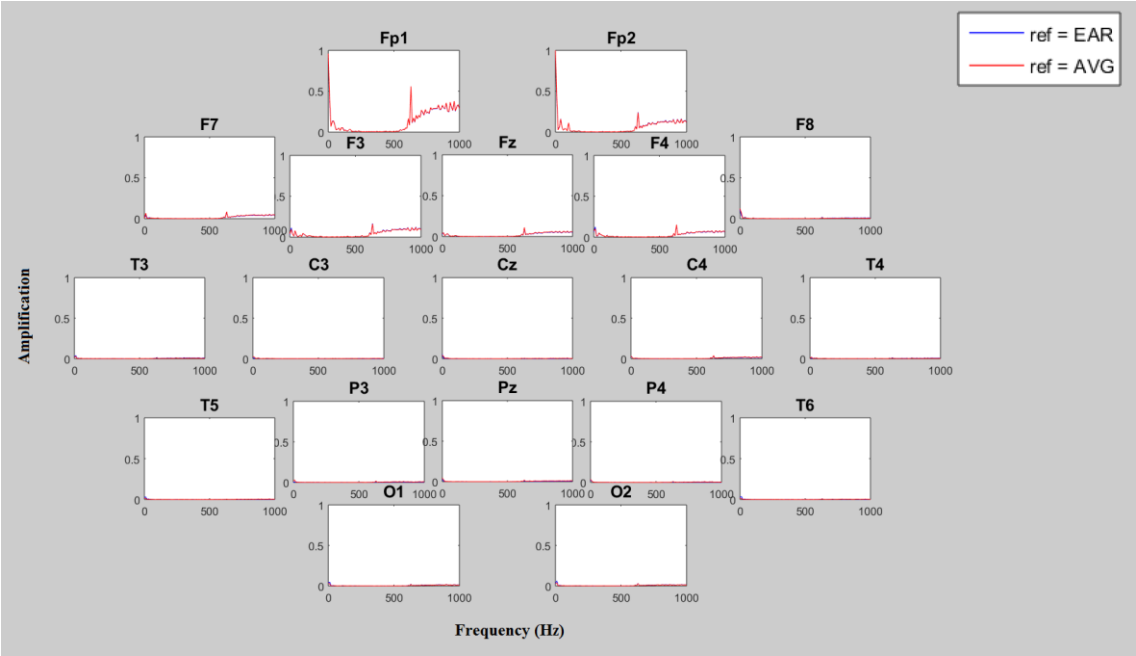

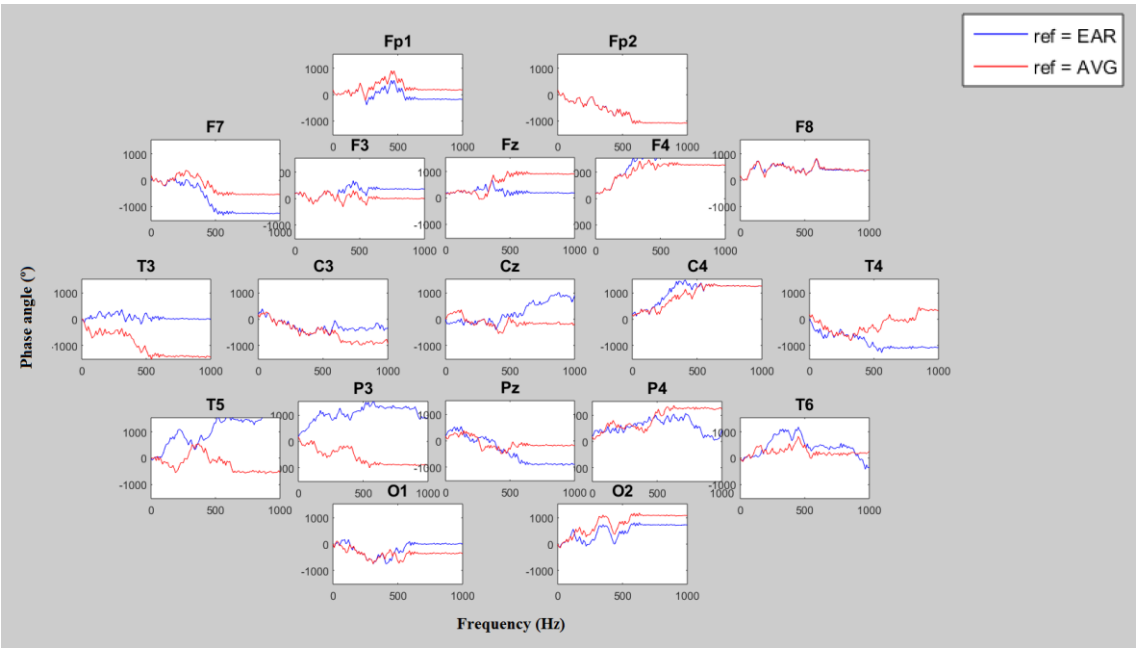

Figure 35. *Normalized amplitude responses and phase responses, when tissues between the left frontalis and the EEG channels have been considered a digital filter. It's clearly seen that the signal attenuates least in some frequency < 100 Hz. Large amplitude responses in frequencies > 500 Hz are non-physiological and occur due to pre-filtering. It's difficult to make conclusions from the phase responses.*

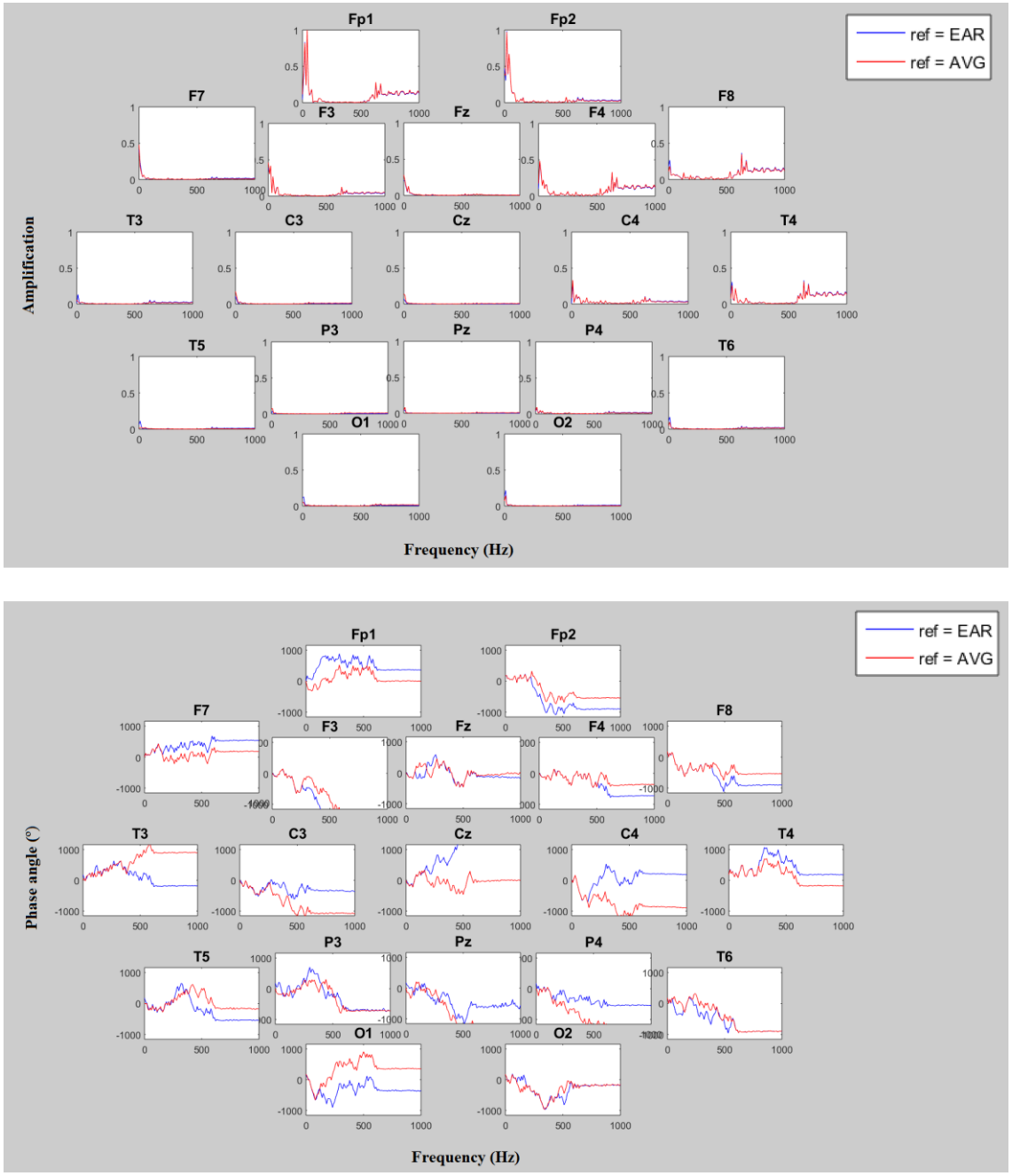

Figure 36. *Normalized amplitude responses and phase responses, when tissues between the right frontalis and the EEG channels have been considered a digital filter. It's clearly seen that the signal attenuates least in some frequency < 100 Hz. Large amplitude responses in frequencies > 500 Hz are non-physiological and occur due to pre-filtering. It's difficult to make conclusions from the phase responses.*

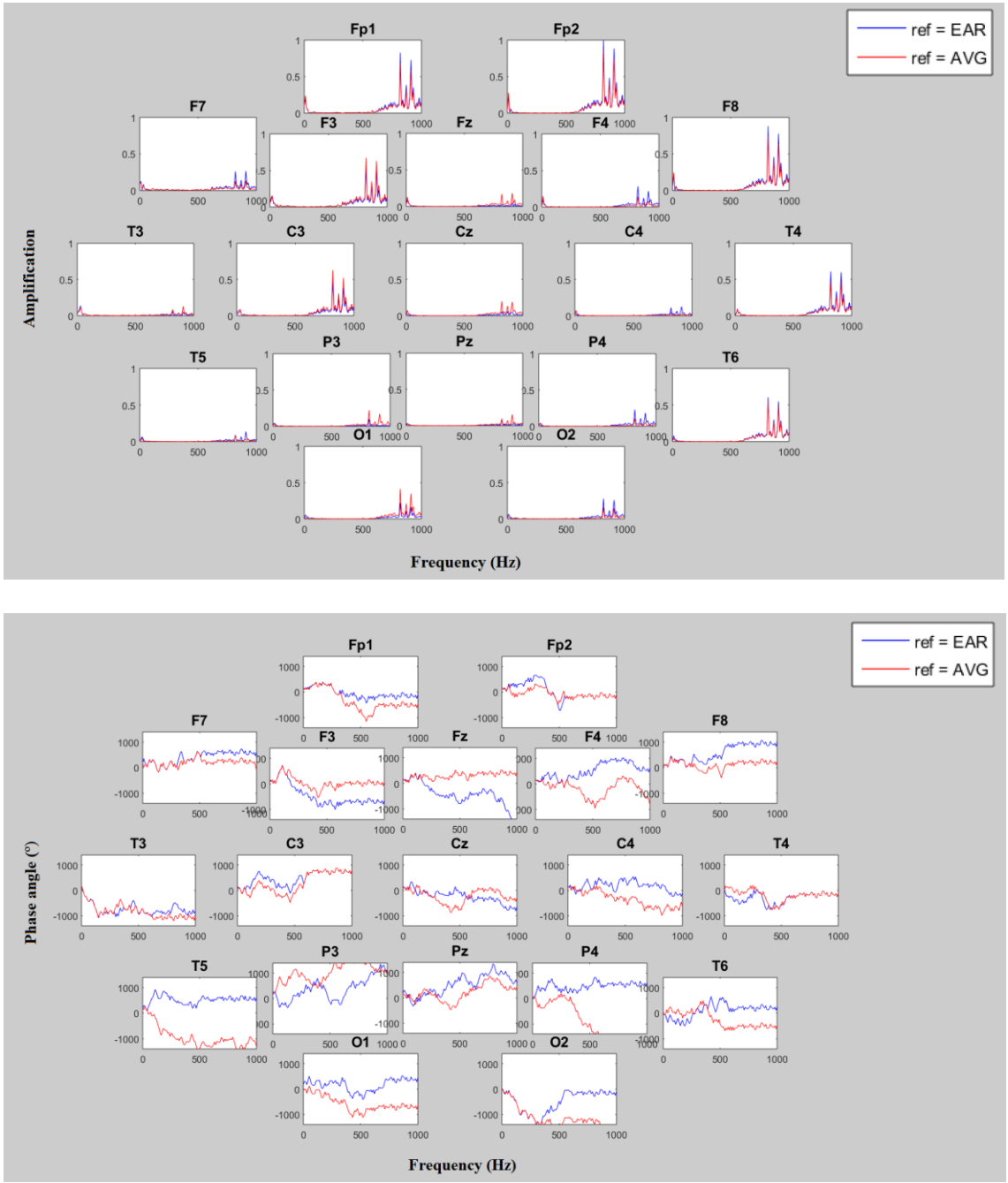

Figure 37. *Normalized amplitude responses and phase responses, when tissues between the left masseter and EEG channels have been considered a digital filter. Large amplitude responses in frequencies > 500 Hz are non-physiological, but occur due to pre-filtering. Also, in some frequency < 100 Hz a peak where signal attenuates least is visible. It's difficult to make firm conclusions from the phase responses.*

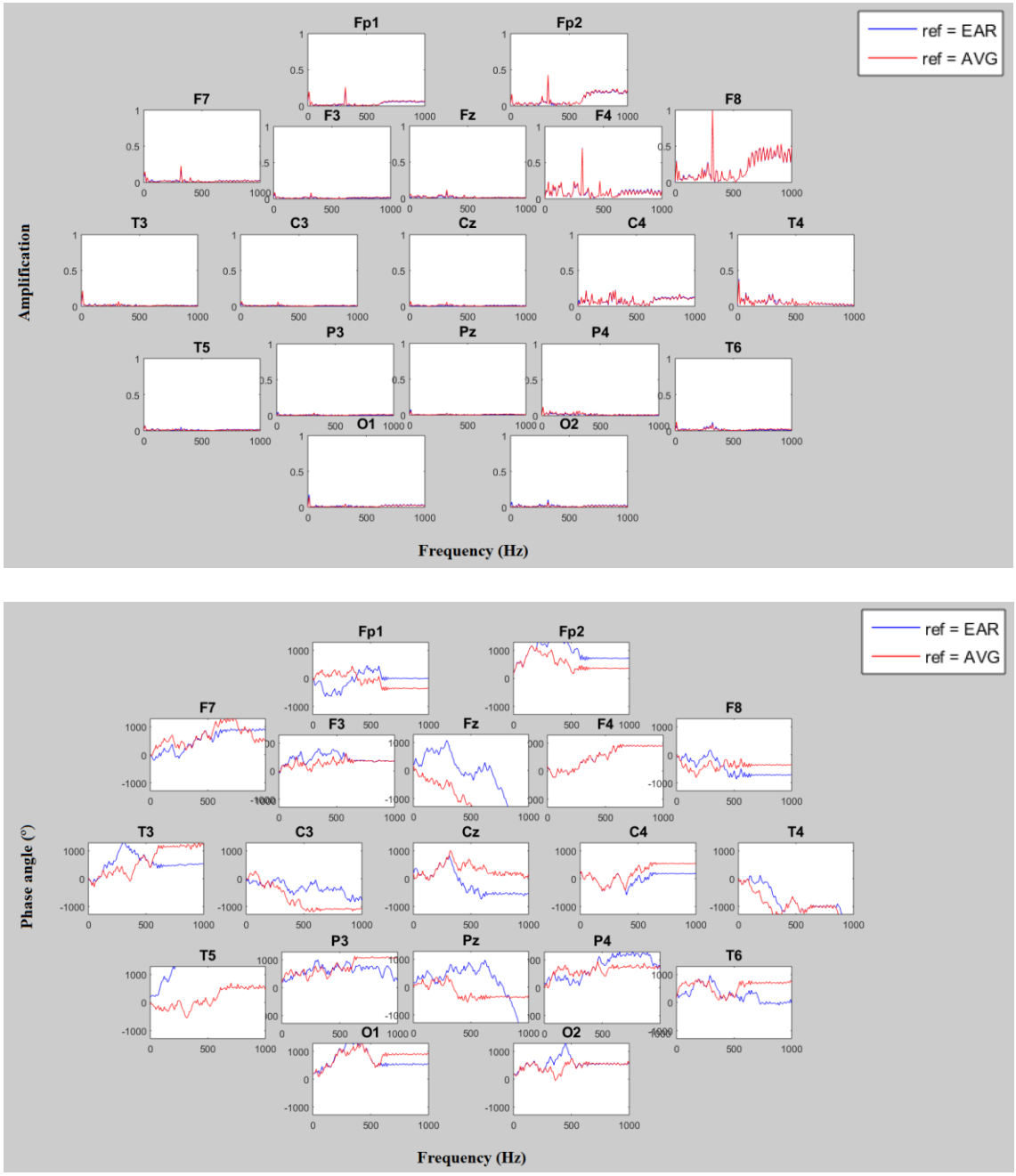

Figure 38. *Normalized amplitude responses and phase responses, when tissues between right masseter and EEG channels have been considered a digital filter. Large amplitude responses in frequencies > 500 Hz are non-physiological, but occur due to pre-filtering. Peak at about 300 Hz is also probably a non-physiological disturbance. Also, in some frequency < 100 Hz a peak where signal attenuates least is visible. It's difficult to make firm conclusions from the phase responses.*

4.4 Simulation

In Figures 39-44 a simulated EMG artefact from all six investigated muscles in EEG channels have been plotted. Both ear-referenced and average-referenced frequency responses have been used. The original simulated EMG signal is shown, too, but because the EMG attenuation coefficient is now known, it's not in scale with artefact signals.

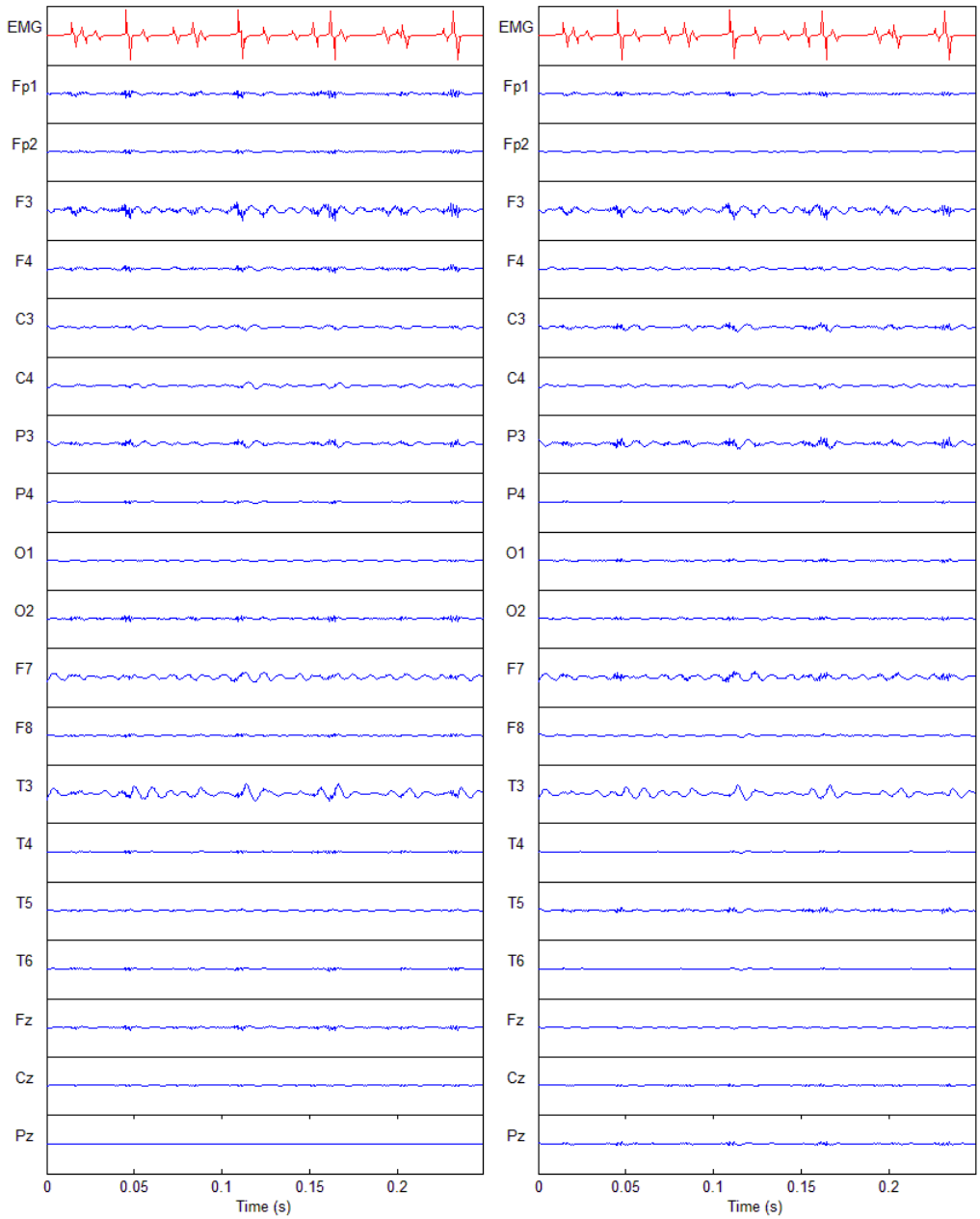

Figure 39. *Simulated EMG artefact from the left temporalis in EEG channels. On the left ear-referenced have been used and on the right average-referenced frequency responses have been used. Signals could be utilized in further studies into how to separate EMG artefact from measured EEG signal.*

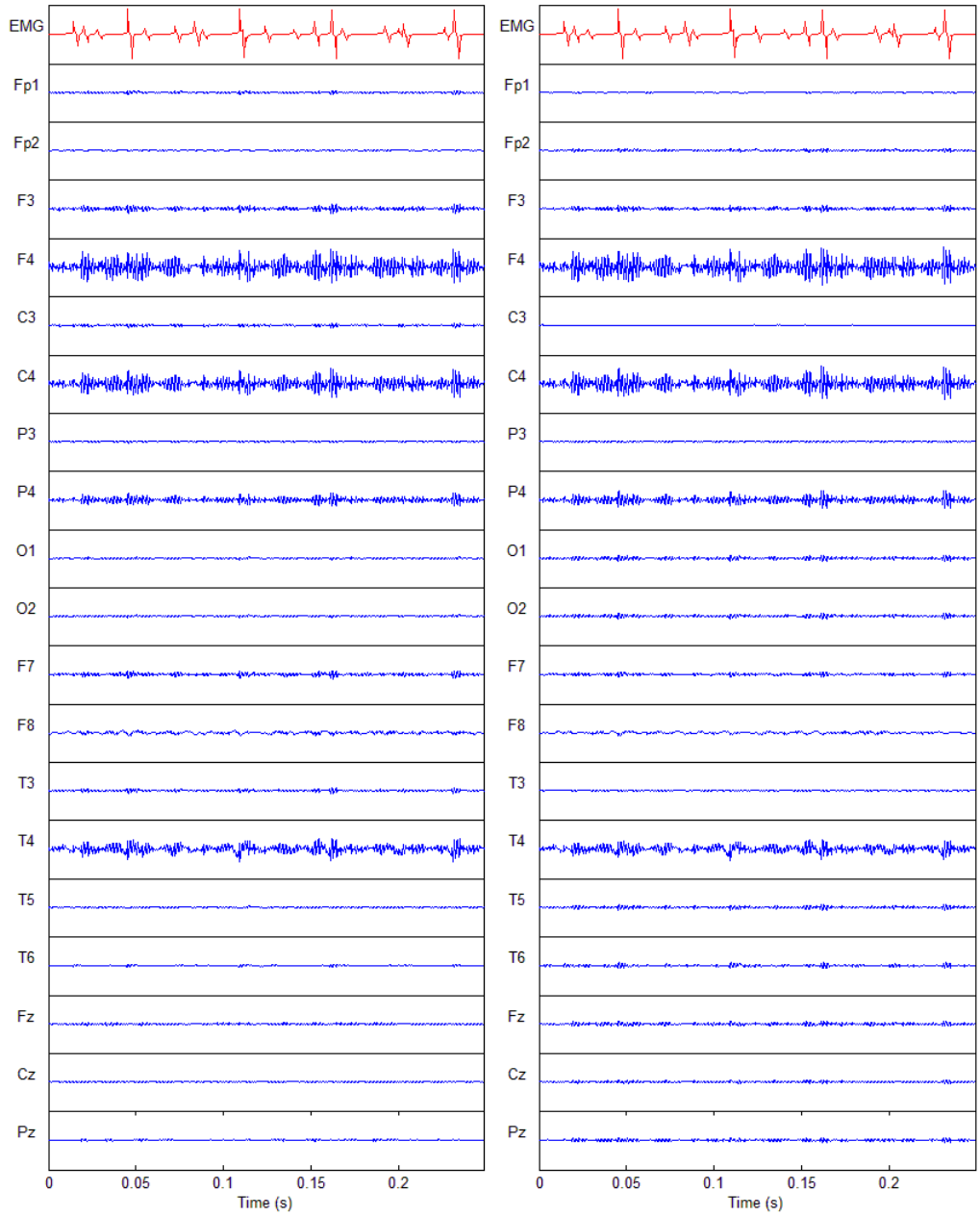

Figure 40. *Simulated EMG artefact from the right temporalis in EEG channels. On the left ear-referenced have been used and on the right average-referenced frequency responses have been used. Signals could be utilized in further studies into how to separate the EMG artefact from measured EEG signal.*

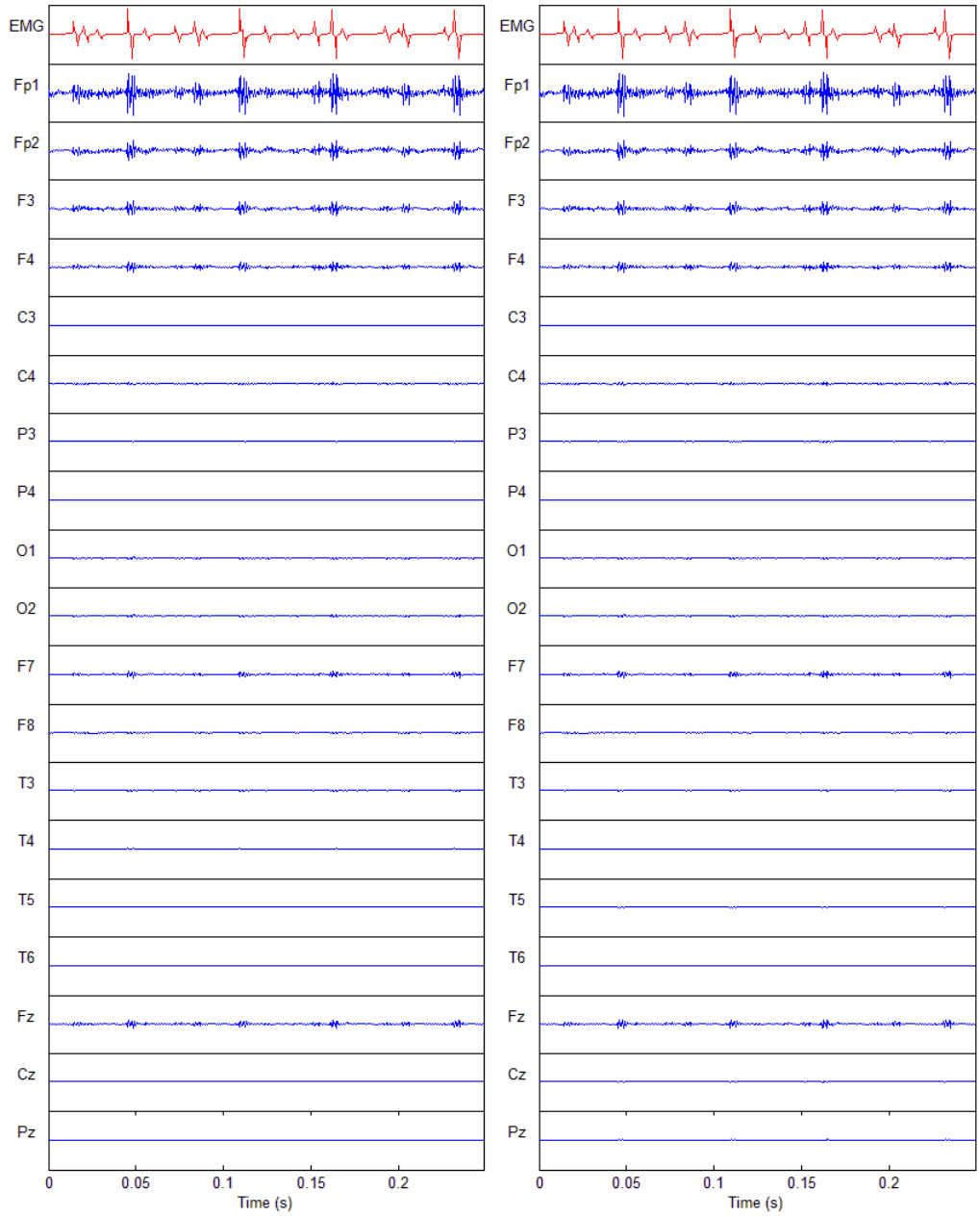

Figure 41. *Simulated EMG artefact from the left frontalis in EEG channels. On the left ear-referenced have been used and on the right average-referenced frequency responses have been used. Signals could be utilized in further studies into how to separate EMG artefact from the measured EEG signal*

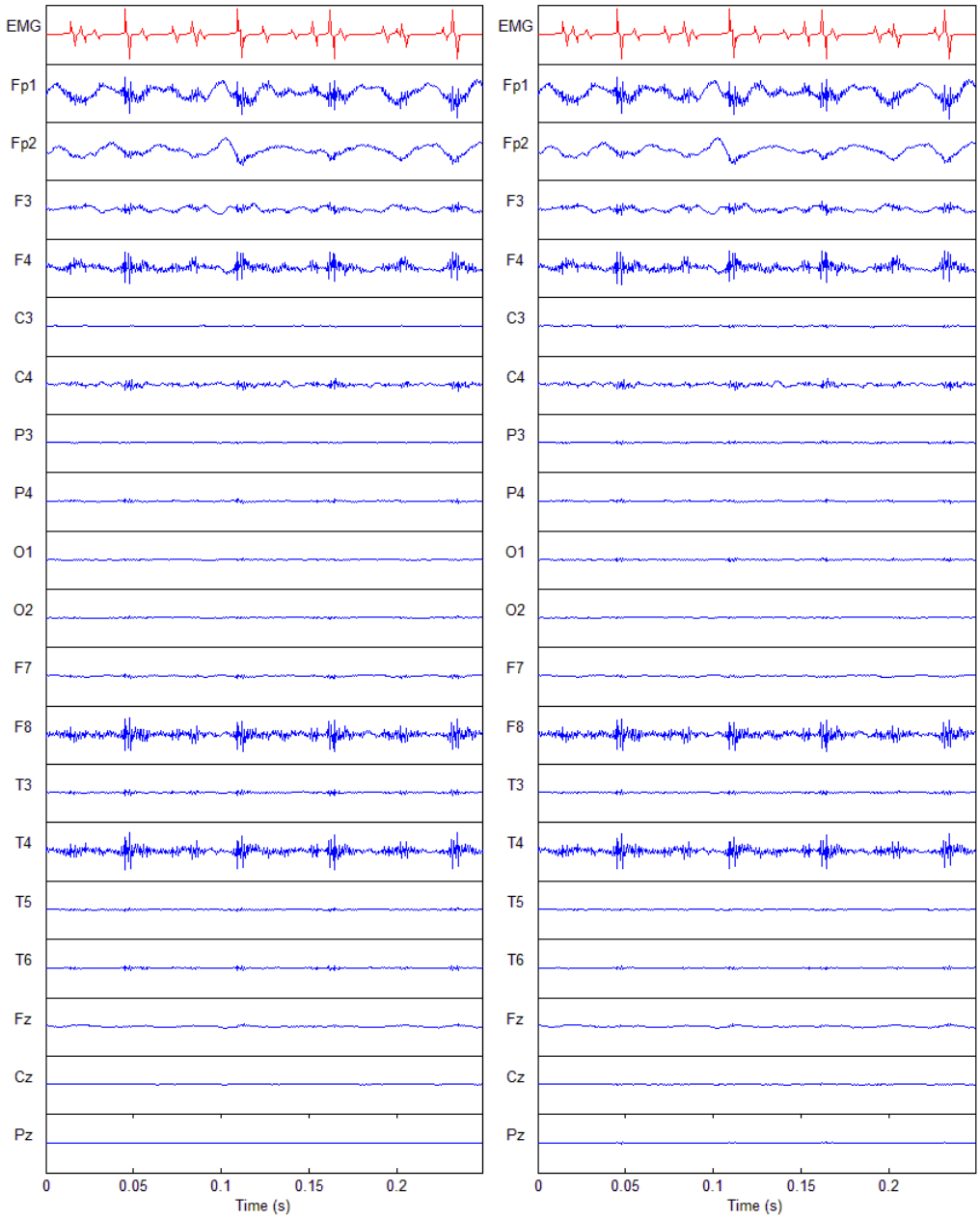

Figure 42. *Simulated EMG artefact from the right frontalis in EEG channels. On the left ear-referenced have been used and on the right average-referenced frequency responses have been used. Signals could be utilized in further studies into how to separate the EMG artefact from the measured EEG signal.*

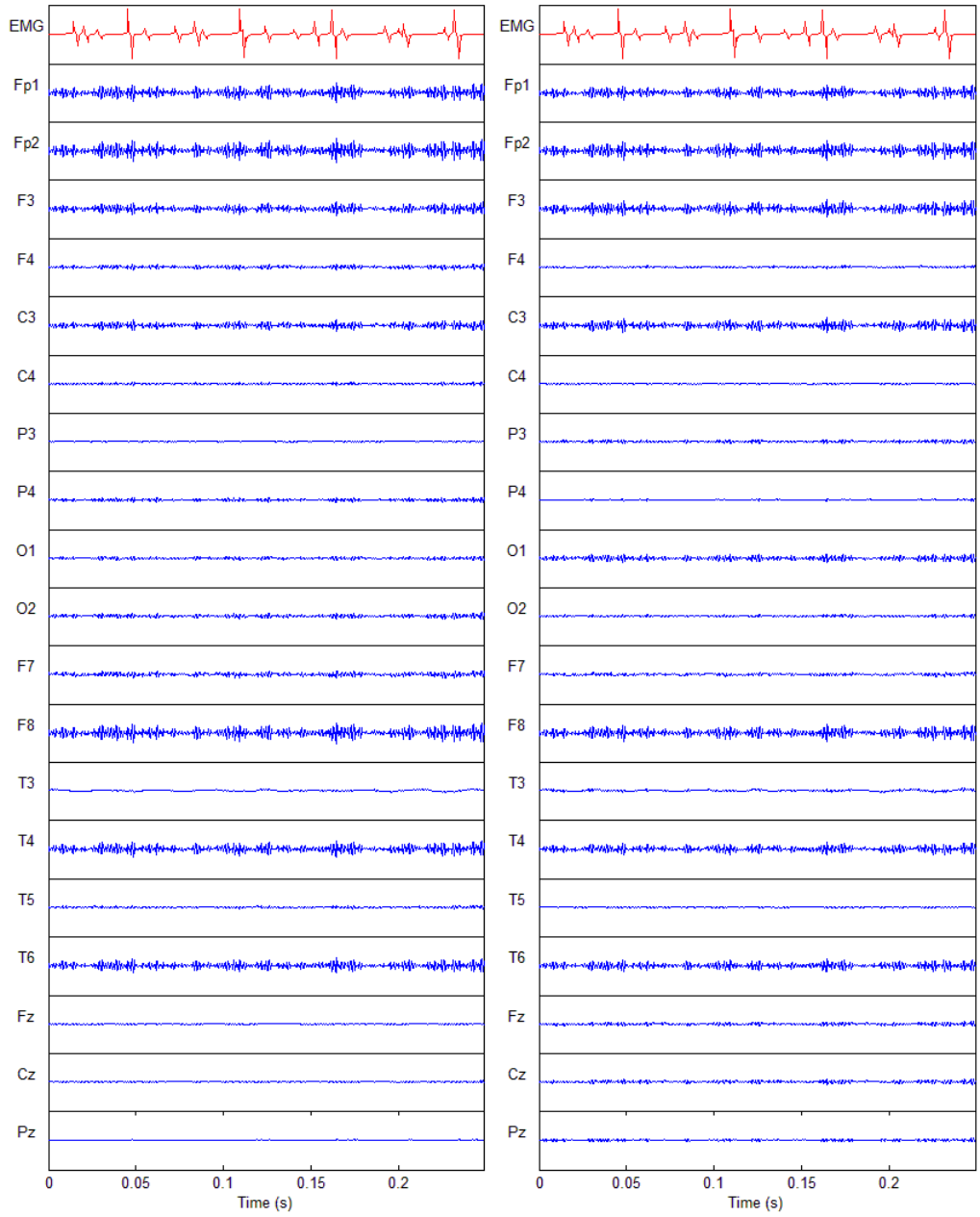

Figure 43. *Simulated EMG artefact from the left masseter in EEG channels. On the left ear-referenced have been used and on the right average-referenced frequency responses have been used. Signals could be utilized in further studies into how to separate the EMG artefact from the measured EEG signal.*

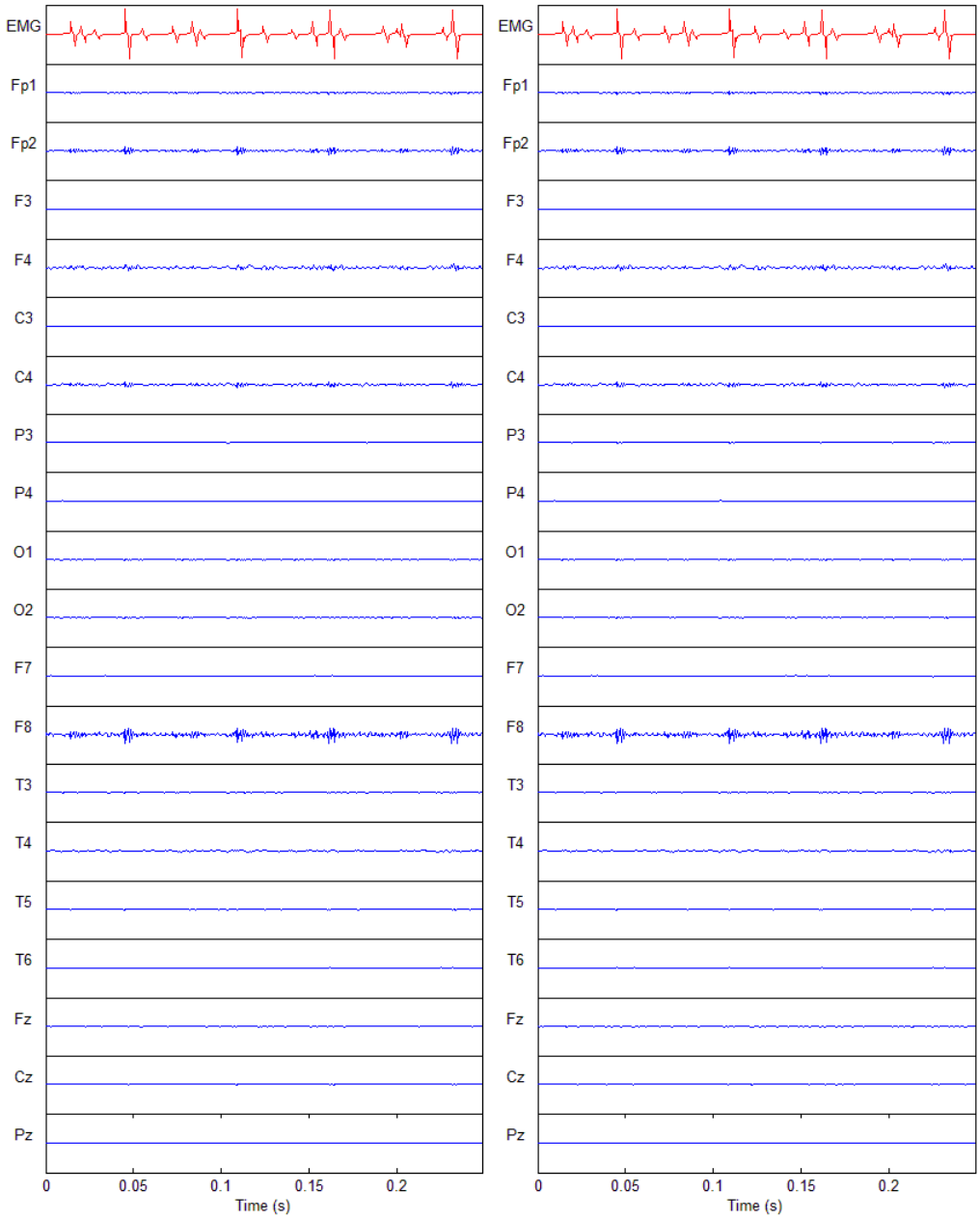

Figure 44. *Simulated EMG artefact from the right masseter in EEG channels. On the left ear-referenced have been used and on the right average-referenced frequency responses have been used. Signals could be utilized in further studies into how to separate the EMG artefact from the measured EEG signal.*

5. DISCUSSION

5.1 MUAP intervals

Interval curves of the facial muscles (in the cases when there were surely no missing MUAPs in the intervals) were observed to be relatively flat as expected. In the curve obtained from the tibialis anterior interval differences were much larger, due to the regulation system of the spinal cord. This information from MUAP intervals could be further used in investigating the separation of the EMG artefact from the measured EEG signal. Part of the interval variation (both in facial muscles and in the tibilias anterior) was probably due to variation of the force used during recording. If this phenomenon were investigated further, force should also be measured. The force has been measured in earlier studies for example from the lip muscles [24], but measuring it from all facial muscles could be difficult.

5.2 Peak-to-peak values

When the strengths of EMG artefacts obtained from EEG recordings are examined, it's noticeable that there are no large differences between ear-referenced and average-referenced values. Average-referenced values can be considered an improvement at least in the case of the temporalis and the masseter, because the EMG source was closer to the other ear. From individual muscles, the dispersion of the EMG artefact from the temporalis muscles appears as expected. It can be clearly observed that the artefact is weak in the midline of the head, because there's no muscle tissue conducting electricity. It was also noticeable that the artefact from the left temporalis in channel P3 is larger than the artefact from the right temporalis in channel P4, even when the EMG was recorded from the same point at both sides. One explanation can be that the head is not completely symmetric. Also, the dispersion of the EMG artefact from the frontalis muscles appears as expected. The artefact from the right frontalis in channels Fp1, C4 and T4 is larger than the artefact from the left frontalis in channels Fp2, C3 and T3, but this can again be explained by head asymmetry. However, in the case of the left masseter, results are not credible. MUAPs of a single motor unit were successfully extracted from the left masseter, but perhaps other muscles activated such that their EMG artefacts were not cancelled in averaging. However, the artefact is largest in channels F7 and F3 which seems correct. Results from the right masseter seem better, but it's strange that the artefact is larger in channel F4 than in channel F8. Signals from

zygomatic channels would have been useful here, because the artefact would have been largest in these channels.

When results computed from the volume conductor model are examined, it's noticeable that in the case of the frontalis and the masseter, the model describes the signal attenuation when distance to EMG source increases reasonably well. In the case of the temporalis, the signal attenuates too quickly. It's difficult to make conclusions from the absolute values, because the EMG attenuation coefficient was not measured. Thus, the model is not suitable for solving the inverse problem. Due to several approximations made in modeling, results differing from recorded values are not surprising. It would have been interesting to see results in the same model, but other parameters defined accurately (conduction velocities of the muscles and direction of the muscle fibers). Also, the metal conductor between the auricular electrodes could have been modeled with potential as a reference, as in recordings. After this, the model itself could be improved by adding tissue types and changing tissue thicknesses and resistivity. The final step could have been taking permittivity (capacitive properties of tissues) into account and using the distributed dipole model instead of single dipoles.

5.3 Frequency responses

When amplitude responses are examined, it's noticeable that in all muscles, the response grows significantly after 500 Hz. This phenomenon is certainly not physiological, and the natural explanation is that the recorded EMG signal had already been filtered with a 500 Hz low-pass filter, but the EEG signals had not. In the right masseter the peak at about 300 Hz is likely another disturbance. However, in all measured muscles some peak at frequencies below 100 Hz is visible, which can be interpreted as a physiological signal. Strangely, the peak measured in the left temporalis is much larger than in the right temporalis. The influence of the 50 Hz electrical artefact should be the same in all cases since the same notch filter was used for all signals. Differences between ear-referenced and average-referenced EEG signals seem to be small.

Interpreting phase responses is difficult. Since the EMG signal had been prefiltered it's not possible to make conclusions regarding responses over 500 Hz. At lower frequencies, the response sometimes becomes positive, which cannot be correct, since an EMG artefact of any frequency cannot occur in EEG channels before the EMG channel. This could originate from noise which has not been cancelled in signal averaging. Differences between ear-referenced and average-referenced EEG signals seem to be much larger than in amplitude responses. Average-referenced responses could be considered better, for the same reason as peak-to-peak values in the time domain. A common trend is that the phase response is reduced when frequency grows,

but it’s difficult to determine whether reduction occurs linearly. This would imply that all frequencies are equally delayed.

From earlier studies where EMG and EEG have been recorded simultaneously, other results can be mentioned, for example from Goncharova et al. [25]. In this study, the spectrum of EMG channels was observed for all frequencies from 0 Hz to over 200 Hz. In the frontalis, there was a peak at 20-30 Hz, and in the temporalis at 40-80 Hz. Attenuation and broadening of peaks was observed in EEG channels. Actual frequency responses between EMG and EEG channels were not calculated. The EMG was recorded with surface electrodes.

5.4 Simulation

Obtained simulated EMG artefacts in EEG channels are not in themselves an actual research result. They could be further exploited, however, for example by adding EEG data, and utilizing another method to separate the EEG data and the EMG artefact. Also, artefacts of single MUAPs could be extracted. Naturally different simulated EMG source signals should be used instead of just a single simulation.

From simulated artefact signals, it’s clear that the aforementioned task would not be easy. In most cases there are no clear EMG spikes, and moreover, it’s impossible to determine in which positions the strongest MUAPs occur in the EMG source signal. However, it seems that it would be easier to recognize the artefact from the frontalis muscle than from the temporalis and masseter muscles. There are no large differences between the artefact signals, regardless of whether ear-referenced or average-referenced frequency responses have been used.

In earlier studies, forming channel-specific EMG artefacts has generally not been attempted, but the same simulated artefact has been added to all EEG channels. For example in the study made by Gao et. al. [38], this type of simulated signal has been used, and investigated canonical correlation analysis (CCA) has been utilized in the removal of EMG artefacts from the EEG.

5.5 Research limitations

A limiting factor in this study was that there was only one test person, and data from a single recording was used. Research aims also should have been defined more clearly, taking into account that it was a Master’s thesis project, whose directive duration is half a year. EMG artefacts are an expansive topic. Research efficiency was also limited by

the fact that many techniques in use today previously unfamiliar to the author of this thesis. Completing additional university courses, for example from the signal processing and biomedical engineering departments would have been useful.

6. CONCLUSIONS

In this Master's Thesis, EMG artefacts from facial muscles in EEG were investigated. The ultimate objective was to determine the frequency bands from the measured EEG signal in which the actual EEG occurs, and in which frequency bands the EMG artefact occurs. Moreover, another goal was to separate the EEG and the EMG if they occur in same frequency band. Determining the muscular origin of the EMG artefact was also a subject of interest.

A comprehensive solution to the objective of separating EMG artefacts from the EEG signal was not directly achieved in the project. Based on the calculated frequency responses, results suggest that a peak occurs at frequencies below 100 Hz, where signal between EMG and EEG channels attenuates least. More recordings, preferably from several test subjects, should be completed. Moreover, it should be verified that the software used hasn't employed any unknown pre-filtrations to signals.

Since simulated EMG artefacts in EEG channels are not in themselves an actual research result, they could be further exploited to separate the EEG data and the EMG artefact. Similarly, frequency responses calculated from several test persons should be used. Different simulated EMG source signals should also be tested.

A conclusion that can be made from the results is that the volume conductor model is not accurate enough to describe EMG conduction inside the head, and thus inappropriate for inverse problems. Instead, a realistic model should be used, and EMG dipoles should be defined more accurately. Exact attenuation coefficient between the EMG needle and the amplifier (if an attenuator is needed) should also be determined.

REFERENCES

[1] F. Netter, Atlas of Human Anatomy, 6th edition, Saunders Elsevier, Philadephia, 2014, 656 p.

[2] E. Marieb, K. Hoehn, Human Anatomy & Physiology, 9th edition, Pearson, San Fransisco, 2013, 1264 p.

[3] L. Sörnmo, P. Laguna, Bioelectrical Signal Processing in Cardiac and Neurological Applications, 1st edition, Academic Press, New York, 2005, 668 p.

[4] J. Partanen, B. Falck, J. Hasan, V. Jäntti, T. Salmi, U. Tolonen, Kliininen neurofysiologia, 1. painos, Kustannus Oy Duodecim, Helsinki, 2006, 784 s.

[5] H. Huttunen, Signaalinkäsittelyn perusteet, Opetusmoniste 2014:1, Tampereen teknillinen yliopisto, Signaalinkäsittelyn laitos, 151 s.

[6] A. Hyvärinen, J. Karhunen, E. Oja, Independent Component Analysis, 1st edition, John Wiley & Sons, Inc., New York, 2001, 481 p.

[7] J. Malmivuo, R. Plonsey, Bioelectromagnetism: principles and applications of bioelectric and biomagnetic fields, 1st edition, Oxford University Press, New York, 1995, 482 p.

[8] R. Kinnunen, Determination of optimal frequency bands for components of the biopotential signals measured from the forehead for assessing the level of sedation, Master of Science Thesis, Tampere University of Technology, 2004, 74 p.

[9] N. Nöjd, Optimal electrode positions for FEMG and EOG measurements, Master of Science Thesis, Tampere University of Technology, 2007, 61 p.

[10] Cephalon, Inc., Nicolet (Nervus) EEG, http://www.cephalon.dk/products/eeg-erp/neeg.

[11] T. van Beelen, EDFbrowser, http://www.teuniz.net/edfbrowser.

[12] B. Kemp, A. Värri, A. Rosa, K. Nielsen, J. Gade, A simple format for exchange of digitized polygraphic recordings, Electroencephalography and Clinical Neurophysiology, 1992 May; 82(5): 391-3.

[13] B. Kemp, J. Olivan, European data format 'plus' (EDF+), and EDF alike standard format for the exchange of physiological data, Clinical Neurophysiology, 2003 Sep; 114(9): 1755-61.

[14] A. Delorme, S. Makeig, EEGLAB: an open source toolbox for analysis of single-trial EEG dynamics including independent component analysis, Journal of Neuroscience Methods, 2004 Mar 15; 134(1): 9-21.

[15] K. McGill, Z. Lateva, H. Marateb, EMGLAB: an interactive EMG decomposition program, Journal of Neuroscience Methods, 2005 Dec 15; 149(2): 121-33.

[16] N. Takano, Noname Bioelectric Field Software, 2001.

[17] Glogster, Neuromuscular junction, http://www.glogster.com/hfandcf/neuromuscular-junction/g-6mdfkot7mj5o76em7nv36a0.

[18] Radiopaedia.org, Facial nerve, http://radiopaedia.org/articles/facial-nerve.

[19] StudyBlue, Action Potential Graph, https://www.studyblue.com/notes/note/n/action-potential-graph/deck/10644361.

[20] StudyBlue, ANTPHY 237 Study Guide, https://www.studyblue.com/notes/note/n/antphy-237-study-guide-2010-11-swan/deck/9736678.

[21] StudyBlue, Face, Neck, Shoulder, Back and Thoracic, https://www.studyblue.com/notes/note/n/face-neck-shoulderback-and-thoracic/deck/4307805.

[22] StudyBlue, Muscle Tissue Etc., https://www.studyblue.com/notes/note/n/muscle-tissue-etc/deck/9748738.

[23] U.S. National Library of Medicine, The Visible Human Project, http://www.nlm.nih.gov/research/visible/visible_human.html.

[24] C. Blair, Firing and contractile properties of human lower lip motor units during sustained isometric contractions, Experimental Neurology, 1988 Feb; 99(2): 269-80.

[25] I. Goncharova, D. McFarland, T. Vaughan, J. Wolpaw, EMG contamination of EEG: spectral and topographical characteristics, Clinical Neurophysiology, 2003 Sep; 114(9): 1580-93.

[26] S. Jung, J. Meklenburg, S. Patrick, Surface Electromyogram Simulator for Myoelectric Prothesis Testing, Liberating Technologies Inc, Holliston, MA, 2010, https://www.wpi.edu/Pubs/E-project/Available/E-project-031210-170006/unrestricted/EMG_MQP_Report.pdf

[27] J. Larsen, C. Norris, J. Cacioppo, Effects of positive and negative affect on electromyographic activity over zygomaticus major and corrucator supercilii, Psychophysiology, 2003 Sep; 40(5): 776-85.

[28] J. Rodriguez-Falces, J. Navallas, A. Malanda, EMG Modeling, http://dx.doi.org/10.5772/50304.

[29] D. Boyd, P. Lawrence, P. Bratty, On modeling the single motor unit action potential, IEEE Transactions on Biomedical Engineering, 1978 May; 25(3): 236-43.

[30] A. Hamilton-Wright, D. Stashuk, Physiologically based simulation of clinical EMG signals, IEEE Transactions on Biomedical Engineering, 2005 Feb; 52(2): 171-83.

[31] Y. Masakado, Motor unit firing behavior in man, The Keio Journal of Medicine, 1994 Sep; 43(3): 137-42.

[32] T. Walsh, P. Ramsay, T. Lapinlampi, M. Särkelä, H. Viertiö-Oja, P. Meriläinen, An assessment of the validity of spectral entropy as a measure of sedation state in mechanically ventilated critically ill patients, Intensive Care Medicine, 2008 Feb; 34(2): 308-15.

[33] T. Walsh, T. Lapinlampi, P. Ramsay, M. Särkelä, K. Uutela, H. Viertiö-Oja, Responsiveness of the frontal EMG for monitoring the sedation state of critically ill patients, British Journal of Anaesthesia, 2011 Nov; 107(5): 710-8.

[34] T. Walsh, K. Everingham, F. Frame, T. Lapinlampi, M. Särkelä, K. Uutela, H. Viertiö-Oja, An evaluation of the validity and potential utility of facial electromyogram Responsiveness Index for sedation monitoring in critically ill patients, Journal of Critical Care, 2014 Oct; 29(5): 886.e1-7.

[35] T. Lapinlampi, H. Viertiö-Oja, M. Helin, K. Uutela, M. Särkelä, A. Vakkuri, G. Young, T. Walsh, Algorithm for Quantifying Frontal EMG Responsiveness for Sedation Monitoring, Canadian Journal of Neurological Sciences, 2014 Sep; 41(5): 611-9.

[36] A. Delorme, T. Sejnowski, S. Makeig, Enhanced detection of artifacts in EEG data using higher-order statistics and independent component analysis, Neuroimage, 2007 Feb 15; 34(4): 1443-9.

[37] R. Chowdhury, M. Reaz, M. Ali, A. Bakar, K. Chellappan, T. Chang, Surface electromyography signal processing and classification techniques, Sensors, 2013 Sep 17; 13(9): 12431-66.

[38] J. Gao, C. Zheng, P. Wang, Online removal of muscle artifact from electroencephalogram signals based on canonical correlation analysis, Clinical EEG and Neuroscience, 2010 Jan; 41(1): 53-9.